The Thesis Committee for Nathaniel Thomas Heathman
Certifies that this is the approved version of the following Thesis

Design and Testing of a Device for Evaluating Rapid Gas Decompression Performance in Elastomers

APPROVED BY
SUPERVISING COMMITTEE:

Supervisor: _____
Richard H. Crawford

_____
Michael Cullinan

Design and Testing of a Device for Evaluating Rapid Gas Decompression Performance in Elastomers

by

Nathaniel Thomas Heathman

Thesis

Presented to the Faculty of the Graduate School of

The University of Texas at Austin

in Partial Fulfillment

of the Requirements

for the Degree of

Master of Science in Engineering

The University of Texas at Austin

May 2019

Abstract

Design and Testing of a Device for Evaluating Rapid Gas Decompression Performance in Elastomers

Nathaniel Thomas Heathman, MSE

The University of Texas at Austin, 2019

Supervisor: Richard H. Crawford

This thesis reports on the design and assessment of a high-pressure test device for the evaluation of rapid gas decompression (RGD) performance of elastomers. RGD damage is a common problem in elastomer seals used in industry applications. RGD results from when gas is diffused in elastomers at high pressures and then is rapidly released from the elastomer when the ambient pressure is lowered rapidly. The resulting damage includes deformation, swelling, blistering, cracking, and, ultimately, failure of the elastomer

To understand the effects of different gas depressurization rates on the elastomer, a commercial off-the-shelf high-pressure test vessel was obtained and modified. Additionally, components for introducing gas, releasing the gas at different rates, heating and temperature control, pressure sensing, data acquisition, and computer control were specified to create a complete test environment. A series of tests was conducted to evaluate the performance of the system based on the NORSOK M710 standard. Damage observed in the test samples is compared to other studies found in the literature. Qualitative correlations between observed damage and test parameters are also proposed. The test

system was demonstrated at pressures to 10 ksi and temperatures to 250°F. The use of an actuated micrometering valve allowed depressurization linearly at 300 psi/min. However, the system as designed suffers from a 10% pressure loss during dwell time, does not provide linear depressurization rates below 250 psi/min, and requires a lengthy calibration procedure. Suggestions for addressing these shortcomings include re-machining the system to accept the factory-specified seal and designing a feedback system to control depressurization.

Table of Contents

List of Tables

List of Figures

1. INTRODUCTION

Elastomer seals are used by virtually every industry spanning the entire globe. Elastomers are used in a variety of situations, from O-ring seals in automobiles to downhole packer devices in oil well production. The many different situations in which elastomers are used opens the door for a large number of failure modes. These failure modes can include, abrasion, chemical degradation, compression set, extrusion, thermal degradation, UV degradation, outgassing, and explosive decompression [1]. Elastomer manufacturers and high-level users are constantly trying to figure out how to get better performance out of their seals. This leads to significant funds being allocated to research outlets every year to address these problems. The research outlined in this thesis takes aim at one of these problems, rapid gas decompression.

1.1 RAPID GAS DECOMPRESSION

Rapid gas decompression (RGD) is the effect of instantaneous depressurization of an elastomer seal after immersing it in high pressure gas at an elevated temperature. RGD can lead to blistering, cracking, and even complete failure of the elastomer seal [2]. The main contributor to RGD is long term exposure to gas at elevated pressures and temperatures. Under these conditions the gas becomes soluble with the elastomer and embeds itself within the polymer chains. Upon instantaneous depressurization, the gas cannot diffuse out of the elastomer quickly, which causes the damage mentioned. RGD

damage to elastomer seals can lead to serious problems in industry applications, whether micro-electronics manufacturing or oil well production.

1.2 PROJECT DOMAIN

The purpose of this project is to construct a testing device to subject elastomers, commonly found in oil well production equipment, to the effects of RGD. It is a continuation of prior testing and based on a previously constructed test device. Successful RGD testing at lower pressures led to the need for a similar device capable of reaching higher pressure. The project sponsor is one of the largest oilfield services companies in the world. Upon completing design and fabrication of the high-pressure testing device, testing was conducted to confirm functionality of the test system and provide examples of the effects of RGD on commonly used elastomers.

1.3 PROBLEM STATEMENT AND APPROACH

As reported in this thesis, the main goal of this project was to construct and evaluate a device for high pressure elastomer rapid gas decompression testing. The process was carried out by assessing the science behind RGD effects, and current industry standards for RGD testing of elastomers. The design process was governed by applying knowledge gained from previous testing to a newly defined set of testing requirements. Design was based on parts provided by the project sponsor and off-the-shelf high-pressure rated components. At the culmination of the design and assembly process, testing was conducted

to evaluate the performance of the assembled test system. With successful completion of the system and evaluation tests, further testing was carried out in accordance with the sponsor's requirements.

1.4 THESIS ORGANIZATION

This thesis is organized into three major chapters, followed by a conclusion. Chapter 2 is a review of the literature, focused on RGD. The scientific basis of RGD is discussed to provide understanding of the mechanisms of RGD. This background informed the design of the experimental test device. Chapter 3 provides details of the design of the device are given. This chapter discusses the equipment provided by the sponsor, initial design drawings for modifying the equipment, additional components sourced for the redesign, final design decisions, construction of the device, and details of the completed device. Chapter 4 discusses experiments conducted with the device, including performance of the device with respect to the specifications, and observations of RGD damage to the elastomer samples tested. Chapter 5 summarizes the research and provides suggestions for improving the system.

2. BACKGROUND & LITERATURE REVIEW

In order to fully grasp the reasons behind RGD damage in elastomers, it is important to fully review the science behind this phenomenon. Rapid gas decompression is classified as an "operational condition during which the applied system pressure is quickly released, resulting in the expansion of absorbed gas damaging elastomer seals" [3]. There are two critical phases to RGD, first the absorption phase, followed by a decompression phase [4]. Both these phases and their respective parameters are important in determining the overall damage to the elastomer. Parameters in the absorption phase include, pressure, temperature, and exposure time. The leading decompression parameters include depressurization rate to atmospheric pressure and the ambient temperature during depressurization. Effects of RGD can include deformation, swelling, blistering, cracking, and complete failure of the elastomer [5]. Examples of observed RGD damage can be seen in Figure 1. The first image shows internal cracking throughout the O-ring. The second image shows cracks rupturing from the interior to the exterior, resulting in complete failure of the O-ring. The third image shows bubbling of the exterior surface of the O-ring.

Figure 1: RGD Damage in O-rings [6]

2.1 Gas Permeability in Elastomers

The driving force behind RGD is gas diffusion into the elastomer during high-pressure exposure. During this exposure there are two predominant effects on the elastomer, first the "plasticization of the polymer matrix leading to increased [polymer chain] movement and an increasing free volume and therefore decreasing glass transition temperature" [7]. The second effect is matrix compression due to the increased hydrostatic pressure. Due to these effects, a volume change of the elastomer is expected, either contracting or expanding depending on which of the two effects is predominant at the applied pressure. Furthermore, the gas permeated elastomer will take on all new thermal and mechanical properties differing from those of the original compound [5].

Gas permeation into the elastomer is defined as a three-step process. First, absorption of the gas molecules into the polymer at the interface, followed by diffusion of the molecules through the polymer, and finally desorption of the permeating species at the opposite interface [8]. Gas permeation is dependent on the free volume of the polymer, as

it is necessary for there to be holes available for the gas to move through the material [9]. Free volume is essentially gaps or microcavities between polymer chains [10] .These microcavities allow a continuous path for diffusion through the polymer. At temperatures above the glass transition temperature, the diffusion process satisfies Fick's first and second laws, shown in the following equations:

$$J = -\omega_v r^{(v-1)} D \frac{\partial c(r,t)}{\partial r} \quad (1)$$

$$\frac{\partial c}{\partial t} = \frac{1}{r^{(v-1)}} \frac{\partial}{\partial r} \left(r^{(v-1)} D \frac{\partial c}{\partial r} \right) \quad (2)$$

where J is the rate of penetrant diffusion; $c(r, t)$ is the local penetrant concentration at a position r and time t; D is the local diffusion constant; ω and v are geometry constants [8]. Through the solution of Fick's equations with associated physical conditions, it is possible to predict the rate of diffusion as well as the gas concentration profile in the polymer. Henry's Law, shown Equation (3), describes the concentration, c, of a gas dissolved in a polymer membrane at the pressure, p, where $S(c)$ is the solubility coefficient.

$$c = S(c)p \quad (3)$$

Solutions and validation of this model can be found in many sources; see [11] for a detailed study of the effects of CO_2 on viscosity of HDPE that directly compares

measured data to that predicted by Fick's model. An even more detailed explanation of the diffusion process can be found in [12]. The application and analysis of this model is sufficient to explaining the mechanisms of gas permeation, however, it alone is not adequate for explaining the evolution of damage that occurs during rapid gas decompression. For this, decompression phase of RGD must also be analyzed.

2.2 Decompression of Gas Permeated Elastomers

The gas molecules that soak into the holes of the elastomer structure during the exposure phase are subject to the same laws of diffusion during the depressurization phase. However, since gas diffusion through the elastomer is a slow process, instantaneous, or even moderately fast depressurization can lead to a non-uniform stress state within the elastomer, deemed as negative hydrostatic pressure [13]. The damage begins as bubbles or blisters in the inhomogeneities; as pressure continues to drop these bubbles rupture, forming cracks that extend to the surface of the elastomer [14].

It is believed that two separate stress fields develop within the elastomer during the depressurization process. The first is a result of the hydrostatic tension acting on the elastomer, and the second is a function of the internal pressure profiles during desorption [15]. The strength of elastomers under negative pressure is very poor and they begin to rupture when a critical pressure is reached. The critical pressure for damage has been computed as a function of the Young's modulus of the elastomer "using the theory of large deformation of incompressible highly elastic materials for two forms of the stored-energy function" [16]. The predicted value for critical pressure was determined to be $5E/6$, where

E is the Young's modulus of the elastomer. The difference in pressures between surface and interior of the elastomer combined with a triaxial stress state are enough to cause serious damage.

There are two types of cracks observed in the RGD process: large axially symmetrical cracks, as in circular cracking in a cylindrical sample, and small, parallel cracks that are always symmetrical about the longest axis of the elastomer [16]. Symmetrical cracking is believed to be a result of the non-uniform stress state within a polymer due to shear stresses generated between the outer and inner regions [15]. Figure 2 provides a visual representation of the stress zones that develop due to the pressure differential. The smaller parallel cracking is most likely attributed to triaxial expansion of the elastomer [17]. According to Briscoe and Liatsis, the elastomer material ruptures due to the hydrostatic tension, but localized stress fields control the direction and location of cracking [16].

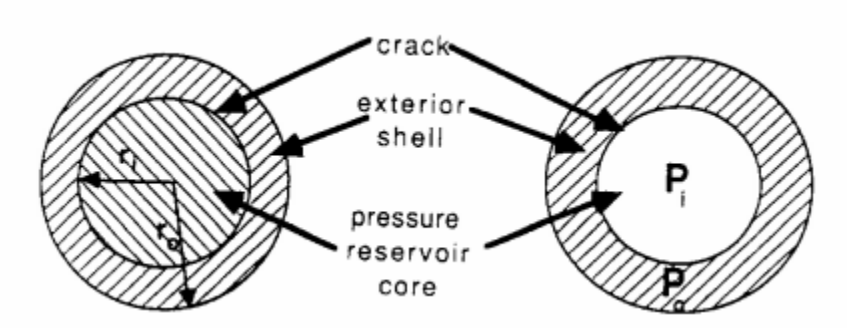

Figure 2: Symmetrical Cracking due to Pressure Differential [16]

The resulting damage can greatly affect elastomer seal performance, or even cause complete failure of the seal. In critical applications this can lead to extended

downtime for seal repair that results in a loss of revenue. To combat this issue, elastomer manufacturers work to create RGD resistant materials. International standards have been developed for qualification of materials to use in RGD applications, and end users have developed guidelines to minimize the effects of RGD damage.

2.3 INTERNATIONAL STANDARDS FOR RGD TESTING

Multiple international standards have been developed for the qualification and testing of RGD resistant materials. These include, NORSOK M710, TOTAL GS PVV 142, NACE TM0297, and ISO 23936-2 [18]. Due to availability and requirements outlined by the project sponsor NORSOK M710 was the focus for RGD testing and evaluation in this research. M710 is a standard developed by the NORSOK Standardization Work Group for international application. It defines the requirements for critical non-metallic sealing materials used in subsea operations. M710 consists of two main parts: the first defines aging test requirements and the second defines requirements for RGD testing. With the absence of any aging required by the project sponsor, the testing portion of M710 is the focus of this section.

The testing section consists of the following guidelines for designing the testing procedure and equipment. Test media must be selected that are representative of that found in the service application. Testing shall be conducted at a temperature close to the service application. Temperature shall be measured through a calibrated thermocouple throughout the test. When performing the test, temperature should be obtained and held for a minimum of 10 minutes before applying gas pressure. Temperature shall be maintained during the

decompression stage of testing. M710 defines a range of tests pressures between 100 and 400 bar, but maintains that a test pressure close to service application should be selected. The test pressure must be measured with a calibrated pressure transducer and reported at the end of the test. Initial exposure period is defined as 72 hours, a period that is adequate for gas to saturate the elastomer; cycles after the initial cycle are to be exposed for 24 hours. If a nonstandard exposure period is used, justification must be presented in the test report. Decompression rate is standardized at 70 bar per minute, but a nonstandard rate can be specified if required by the service application. The number of cycles shall be 1, 5, 10, or 30. The test vessel used must be rated for operation at the specified pressure and temperature. Furthermore, the ratio of the vessel's volume to the total volume of the samples should be greater than 25:1. Testing should be conducted on elastomers in unconstrained and constrained manners. For O-rings a standard compression of 20% of the original section diameter should be used. [19]

In addition to the guidelines for testing and test apparatus construction, M710 provides a comprehensive method of examining the elastomers for RGD damage. The system involves sectioning the tested elastomer and applying a 0-6 rating to the observed damage. The rating system can be seen in Table 1.

Description	Rating #
No internal cracks, holes or blisters of any size	0
Few small internal cracks (6 or less), each less than 1 mm in size	1
More than 6 small internal cracks, each less than 1 mm in size	2
Few internal cracks (6 or less), each less than 4 mm in size but with at least one crack larger than 1 mm	3
Many internal cracks (more than 6) in the size range 1-4 mm	4
One or more internal crack larger than 4 mm	5
Complete separation of the seal into fragments	6

Table 1: NORSOK M710 Damage Rating System [19]

The NORSOK guideline was used as a basis for designing experiments for the testing carried out in this research. At the conclusion of testing, all elastomer samples were sectioned and rated for damage based upon the 0-6 damage scale. This type of testing procedure and rating system aligns directly with the requirements of the project sponsor.

The background research presented provides an \ understanding how gas diffuses into elastomers and subsequently causes damage during rapid decompression. Furthermore, the analysis of NORSOK M710 gives a starting point for designing high pressure RGD equipment and developing tests to gauge its performance. This information informed the design process presented in the next chapter, which includes descriptions of the provided equipment, design decisions, specified components, and construction of the device.

3. DESIGN AND CONSTRUCTION OF TESTING EQUIPMENT

3.1 FIXTURE REQUIREMENTS

The first step in the design process was to work with the project sponsors and define the exact requirements for the new device. The device had to be capable of holding nitrogen gas at pressure and an elevated temperature overnight, then depressurizing in a linear controlled rate back to atmospheric pressure. Critical parameters included a working pressure of 10,000 psi, depressurization rates between 5 psi/min to 1000 psi/min, and a gas temperature range of 75°F-400°F. Other requirements included remote operation, an over-pressure failsafe, and minimizing device size. Testing gas was set as 99.9% pure Nitrogen. A summary of the requirements is shown in Table 2.

Major Requirements
10,000 psi Working Pressure
5 psi/min - 1,000 psi/min Depressurization Rates
75°F-400°F Temperature Range
Secondary Requirements
Remote Operation
Over-pressure Failsafe
Minimize Footprint

Table 2: Summary of Design Requirements

3.2 PRESSURE VESSEL

At the beginning of the test device design process, a cart mounted pressure vessel was provided by the project sponsor on which to base the design of the system. The vessel was purchased used from an outside test lab. The vessel was identified as a High Pressure Equipment Company (Erie, PA, USA) confined gasket closure reactor with a working pressure of 13,000 psi at 100°F and a maximum hydrostatic test pressure of 19,500 psi [20]. The vessel has an approximate volume of 70 in^2 with two inlet/outlet ports and a thermocouple well for temperature monitoring. Figure 3 provides a picture of the previously described vessel. See Appendix A for a design drawing of the pressure vessel.

Figure 3: GC-17 Pressure Vessel [20]

The vessel came pre-mounted on a rolling steel cart, which proved to be ideal basis for the design of the system. The cart has three shelves, measuring 27.75” between the top most and bottom levels and 24” length and width. Included with the cart assembly are two resistance heating bands which wrap around the pressure vessel. Figure 4 provides a rendering of the cart and pressure vessel assembly.

Figure 4: Pressure Vessel and Cart Assembly Rendering

3.3 HYDRAULIC DESIGN

After fully analyzing the provided pressure vessel and carefully considering all given requirements, a design plan was developed. With the generous amount of space on the cart assembly, the initial idea was to mount all the required system components directly on the cart, leaving it self-contained and mobile. For the system to meet its functional requirements, multiple critical components were chosen. The inlet and outlet gas flow are controlled by remote actuated ball valves. Gas depressurization rates are controlled by a remote actuated micro-metering valve on the outlet side of the pressure vessel. Pressure is

recorded using a high-pressure transducer. Safety is ensured by using a pressure set relief valve as the primary over-pressure protection and a burst disk as a back-up. Working pressure is achieved using a high-pressure gas booster. All components are connected to the pressure vessel using high-pressure stainless-steel fittings. After identifying the necessary system components, initial draft design sketches were created (see Figure 5).

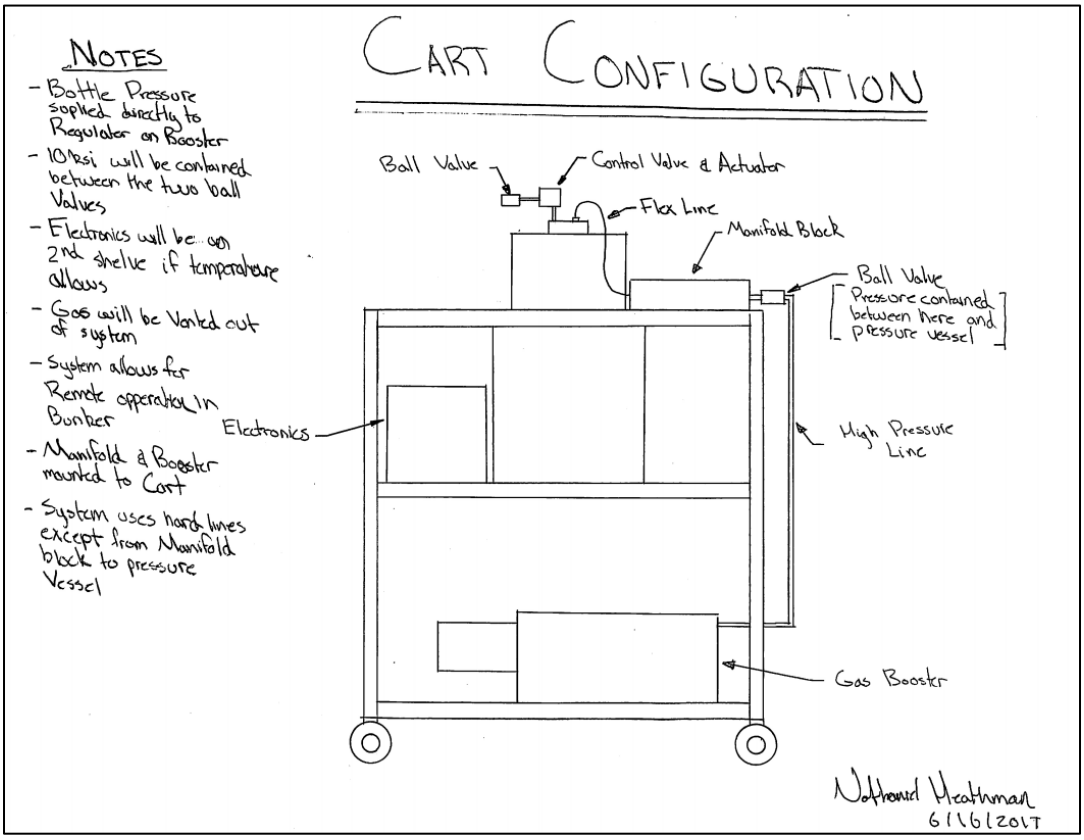

Figure 5: Cart Configuration

The first design iteration contained four major components mounted on the pressure vessel cart assembly. A high-pressure booster is located on the first level of the cart with a

pressure line supplying gas to the inlet manifold block after passing through an on/off ball valve. The inlet manifold block houses all necessary data acquisition and safety components such as the pressure transducer, analog pressure gauge, relief valve, and burst disk. Flex line connects the manifold to the pressure vessel. Outlet flow is controlled via the actuated metering valve and on/off ball valve. All electronics are housed on the 2nd level of the cart.

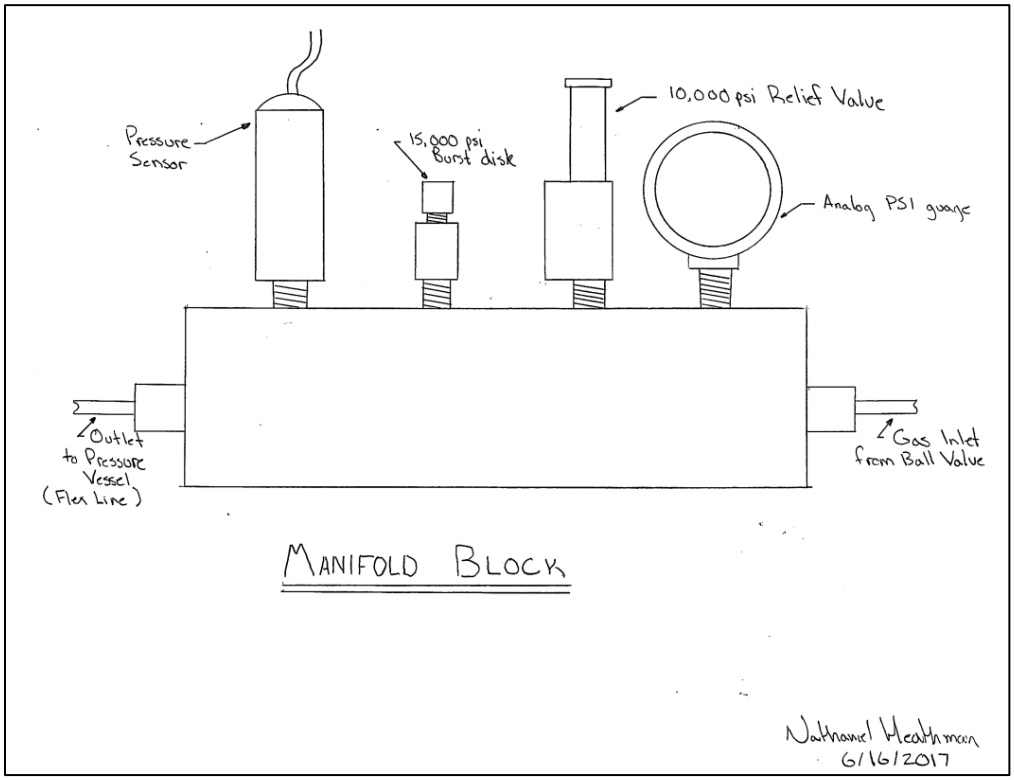

Figure 6: Manifold Block

The use of a manifold block simplifies the placement of all necessary inlet side components into one compact, easy-to-mount, device. The required inlet side components

included a pressure transducer capable of reading pressures up to 10,000 psi at a temperature up to 400°F. In order to ensure equipment operator safety, a standard analog pressure gauge is mounted in series with the transducer. The pressure relief valve is set to open right above the working pressure. The burst disk is selected to fail at the maximum rated working pressure of the vessel.

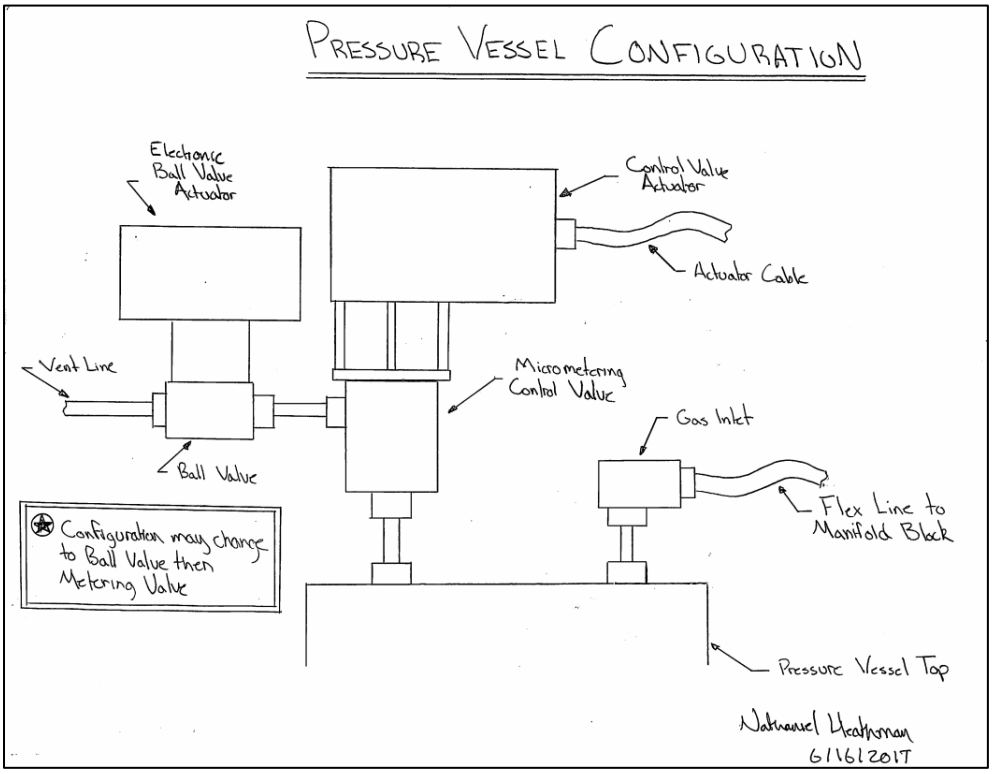

Figure 7: Pressure Vessel Configuration [20]

The gas inlet side is connected to the manifold block with a flex line to aid in pressure vessel assembly. The gas outlet side is connected directly to the metering valve to reduce gas flow disturbances. The on/off ball valve is placed directly after the micro

metering valve so that gas flow does not surge when opening the valve. After receiving the pressure vessel cart assembly and completing the first iteration design, all the necessary components were sourced from suppliers and a computer aided design model was developed.

3.4 Final Component Selection

The first task was to identify and procure long lead time, high cost components. These included the high-pressure booster, electronic actuated ball valves, relief valve, pressure transducer, and metering valve actuator. Beyond this, all the specified components were virtually assembled in SolidWorks (Dassault Systèmes SolidWorks Corporation, Waltham, MA, USA) to assess their sizes and mounting options with regard to the pressure vessel cart assembly.

Immediately, it was determined that the price and limited available mounting space made a custom machined manifold block infeasible for the design. The design process was changed such that all high-pressure components are mounted individually on the cart. Due to concerns about high levels of vibration and proximity of the electronics on the second level next to the heating bands, the pressure booster was relocated to the floor next to the cart assembly and connected to the inlet side of the manifold system with a flex line. All system control electronics are mounted on the lowest level of the cart. To keep all pressure contained within the system during testing, the plumbing is arranged to bleed pressure between the high-pressure booster and inlet ball valve. A solenoid valve is attached to the fill line to bleed high-pressure gas from the booster through a needle valve once the inlet

ball valve is closed. For consistency, all purchased high-pressure components use a ¼" high-pressure coned fitting that matches those found on the top of the pressure vessel. The use of ¼" fittings throughout the system also minimizes overall component size while maintaining adequate gas flow.

The first item acquired was the gas booster because it was anticipated to have the longest lead time. A gas booster is responsible for increasing the gas media from the bottle or other supply, usually 500–2500 psi, to high pressures. In the standard form, gas boosters are driven by a low pressure compressed air source, such as 90 psi shop air. Multiple gas booster manufactures were considered, but after comparing prices, lead time, and performance, a Haskel AG-152 single acting single stage gas booster was chosen (Haskel International, Inc., Burbank, CA, USA). This booster is capable of providing a maximum 20,000 psi outlet pressure with a minimum 250 psi supply pressure, using only 90 psi supply air source [21]. This booster supplies more than the necessary amount of gas pressure for this project and foreseeable future projects. See Appendix A for a dimensioned drawing and Figure 9 for a representative view of the booster.

Figure 8: Haskel AG-152 [21]

After assessing high pressure micro-metering valve options, an industry standard design in high-pressure valves for fine flow control was identified. The Parker-Autoclave (Erie, PA, USA) option has a maximum pressure of 60 ksi, optional temperature range up to 1200°F, and a C_v range between 0 and 0.004, where C_v is the flow coefficient of the valve [22]. Based on prior experimentation, it was determined that this C_v range can accommodate the desired depressurization rates. The chosen valve is model number 30VRMM4812TGK (see Figure 9). This valve has a maximum pressure of 30 ksi, ¼" fittings, and PTFE glass packing rated to 600°F.

Figure 9: VRMM Micrometering Valve [22]

For metering valve control, a Hanbay MCL series actuator was sourced for fine control over valve adjustment (Hanbay, Inc., Virginia Beach, VA, USA). The MCL actuator is a fully adjustable, gear driven, brushless, motor-powered device. It has a torque range of 18 – 60 in-lbs, speed range of 1-5 sec per rotation, and positioning precision of +/-0.25° [23]. The actuator is powered with 12-24VDC, controlled via a 1-5VDC input, and has adjustments for torque, speed, and total turn count by means of internal dip switches. See Appendix A for the M-series actuator data sheet.

Figure 10: Hanbay MCL Actuator [23]

Because of the high testing temperature requirements, the pressure transducer options were narrowed considerably. The only available offerings identified were from Emerson (St. Louis, MO, USA), SensorsONE (Oakham Rutland LE15 0AW UK), Honeywell (Morristown, NJ, USA), and OMEGA Engineering (Norwalk, CT, USA). Based on price, lead time, and functional requirements the Omega PX1004 sputtered thin-film high-temperature pressure transducer was selected (see Figure 11). This transducer is capable of reading pressures up to 10 ksi at temperatures of 450°F with a static accuracy of +-0.25% [24]. Because the transducer comes unamplified, a signal conditioner is used to amplify the output signal. By recommendation, an Omega IN-UVI series inline amplifier [25] was also purchased to provide a 0-5V output signal from the transducer. Both items were sourced directly from OMEGA Engineering and were delivered as a calibrated and tested set. See Figure 12 for a picture of the IN-UVI Amplifier.

Figure 11: Omega High Pressure Transducer [24]

Figure 12: Omega DMD-17 Amplifier

To safely contain all pressure within the system during testing, Parker Autoclave ball valves with DC powered electric actuators were chosen. Ball valves were sourced from Autoclave Engineers 2-way series offerings; the specific models of valves chosen were a 2B4S20H4 with a 0.094” orifice and a 2B4S20H9 with a 0.188” orifice. A larger orifice size was chosen for the exhaust side to avoid restricting flow after the metering valve. Both of these valves are rated up to 20ksi and were optioned to withstand 500°F [26]. The actuators chosen are Autoclave’s 24VDC powered EO3s (see Figure 13).

Figure 13: Autoclave Engineers EO3 Actuator [23]

Two forms of mechanical over-pressure protection are utilized: a relief valve set at maximum working pressure and a burst disk set above working pressure, but below the minimum rated pressure for system components. The relief valve chosen is an Autoclave 15RVP9072-HT (see Figure 14). The 15RVP series valve is a metal seat relief valve rated to 15 ksi and with the high temperature option, rated to 750°F [27]. The relief valve is specified to open at 10 ksi, the maximum working pressure of the system. For a final fail-safe against an over-pressure situation, an Autoclave universal safety head is used in conjunction with a rupture disk. The safety head chosen is a CS4600 with a P-7048 3/16 flat Inconel rupture disk set to fail in the 11,925-13,250 psi range [28]. This allows pressures of 10 ksi to be safely reached, and in the event of an over-pressure situation combined with relief valve failure, the rupture disk will fail before pressures reach maximum ratings for any components in the system.

Figure 14: Autoclave Engineers Relief Valve [27]

To keep all pressure contained within the system during testing, the fill line between the gas booster and inlet ball valve must be bled after every fill. To accomplish this a solenoid valve is attached to the fill side before the ball valve. The solenoid valve chosen is an Omega SVH-111 rated to 10 ksi and powered by 110VAC (see Figure 15). The valve bleeds pressure through an Autoclave 60VM4072 needle valve (See Figure 16) to slow the gas flow to avoid any ill effects of venting unmetered high-pressure gas straight to the atmosphere.

Figure 15: Omega High Pressure Solenoid Valve [29]

Figure 16: Autoclave Engineers Needle Valve [30]

The primary system components are connected and mounted with stainless steel Autoclave high pressure fittings. Many different fittings are used, such as tees, elbows, and unions, all connected by coned and threaded tubing of various lengths. Several components require adapters, such as the pressure transducer, relief valve, larger ball valve, and inlet pressure relief valve. Autoclave offers adapters for virtually any situation and finding fittings to mount these components was not difficult.

With all the primary components specified, attention was turned to creating a final design for the system in Solidworks. This involved final decisions on tubing lengths, fitting quantities, component mounts, and greatly aided in identifying any foreseeable problems with assembling the system. See Appendix B for a bill of materials of all components ordered.

3.5 FINAL DESIGN

CAD layouts were critical in making final design decisions for the system. With the pressure vessel and cart already modeled, the next step was to insert each component and their coupled fittings into the assembly. The components were laid out on the cart according to the previous design. CAD renderings of components available from Autoclave Engineers were used, as well as custom modeled parts. After placing all parts within the confines of the cart and available parts, a final design was reached. A rendering of the final design can be seen in Figure 17. The left-hand rendering shows the difference in exhaust and intake, while the right shows orientation to the cart.

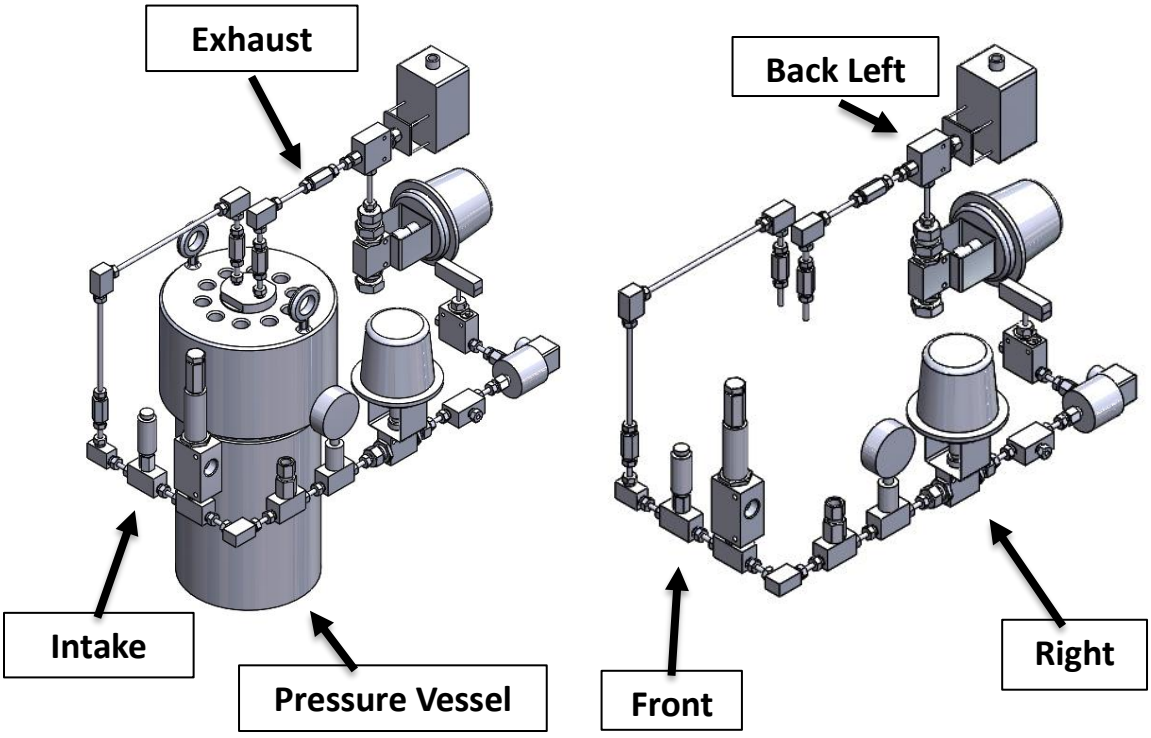

Figure 17: Hydraulic System Design

The design is modularized into separate intake and exhaust manifolds, taking up three sides of the cart. The intake manifold consists of the front and right-side components. The exhaust side components are contained on the back-left side of the cart. All components on the intake side are connected with 2.75” coned and threaded tubes to minimize space. The exhaust side is mounted vertically to save room on the cart and minimize flow obstructions. The components on the exhaust side are attached using tubing lengths appropriate for the space available.

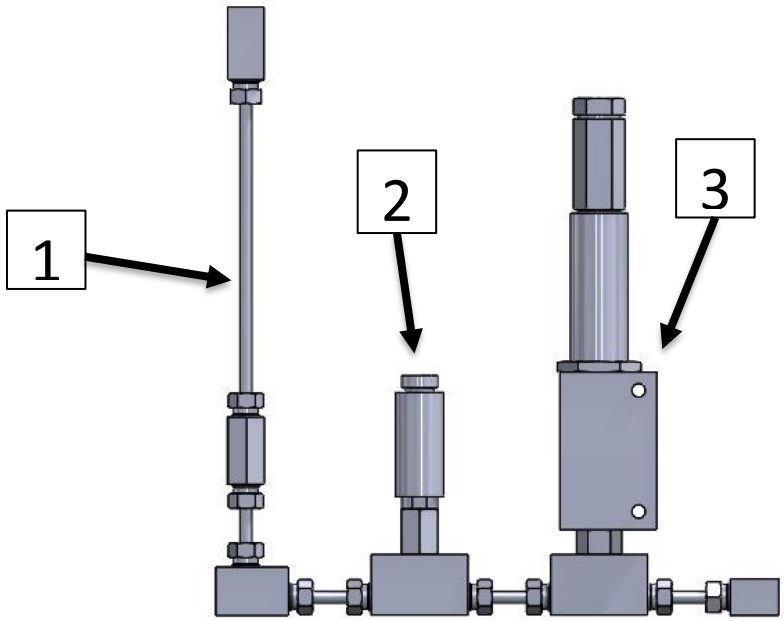

Figure 18: Front Side Components; Item 1: Pressure Vessel Connection Item 2: Pressure Transducer, Item 3: Relief Valve

Figure 18 shows the front side of the intake manifold. Item 1 is the tubing that connects to the top of the pressure vessel. Item 2 is the Omega PX1004 pressure transducer, which connects to the manifold via a high-pressure tee and flared high pressure fitting end to ¼" male high-pressure fitting adapter. It is placed closest to the pressure vessel in order to minimize possible pressure discrepancies between the intake and exhaust side. Item 3 is the Autoclave relief valve that connects to the manifold using a tee and a 9/16" to ¼" high pressure fitting adapter.

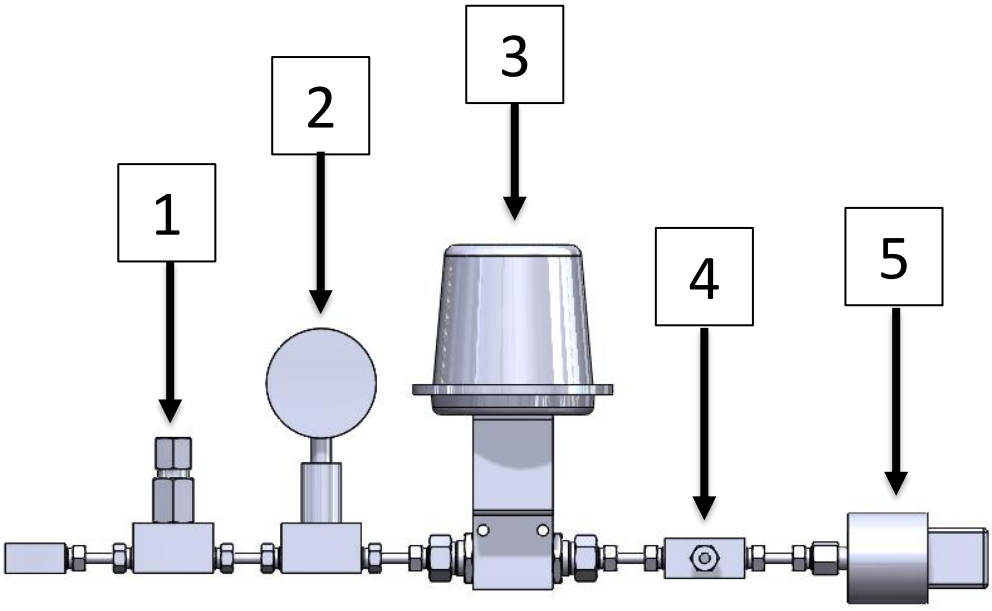

Figure 19: Right Side Components; Item 1: Safety Head, Item 2: Pressure Gauge, Item 3: Ball Valve, Item 4: Gas Inlet Tee, Item 5: Solenoid Valve

Figure 19 shows the right side of the intake manifold. Item 1 is the Autoclave safety head and burst disk assembly, which is connected to the manifold via a high-pressure tee.

Item 2 is the analog pressure gauge, which is connected to the manifold using a high-pressure tee. Item 3 is the ¼" ball valve and EO3 actuator. During testing all pressure is contained to the left of the ball valve. Item 4 is the gas inlet tee that connects to the outlet of the gas booster. Item 5 is the Omega SVH-111 solenoid valve. Not seen is the needle valve attached to the solenoid valve that meters the gas flow from the inlet fill line during bleeding.

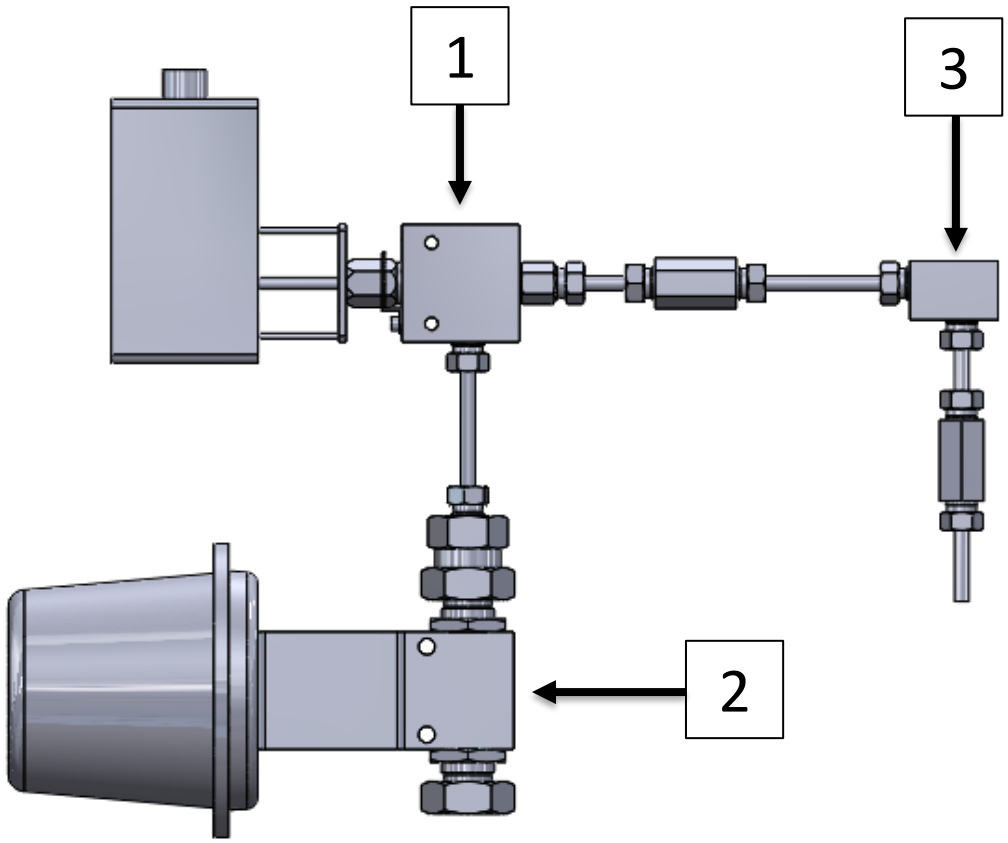

Figure 20: Exhaust Side Manifold; Item 1: Micrometering Valve, Item 2: Ball Valve, Item 3: Pressure Vessel Connection

Figure 20 shows details of the exhaust side manifold. Item 1 is the Autoclave micro-metering valve and attached Hanbay MCL actuator. Item 2 is the 9/16” Autoclave ball valve and EO3 actuator. Item 3 is the tubing connected to the pressure vessel. During testing all pressure is contained upstream of the ball valve.

After arranging all the parts on the cart, a series of mounts was designed to support the intake and exhaust manifolds. On the intake side, mounts were designed for the relief valve, safety head, ball valve, solenoid valve, inlet tee, and the elbow connected to the pressure vessel tubing. All the mounts on the intake side are machined out of aluminum and bolted directly to the cart. The vertical arrangement of the exhaust manifold made mounting more challenging. To provide adequate support to mount the exhaust manifold components, 40 mm T-slotted extruded aluminum is used. Parts are designed to attach the ball valve and metering valve to the extruded aluminum. The extruded aluminum is braced by diagonal struts and then bolted to the table in three places.

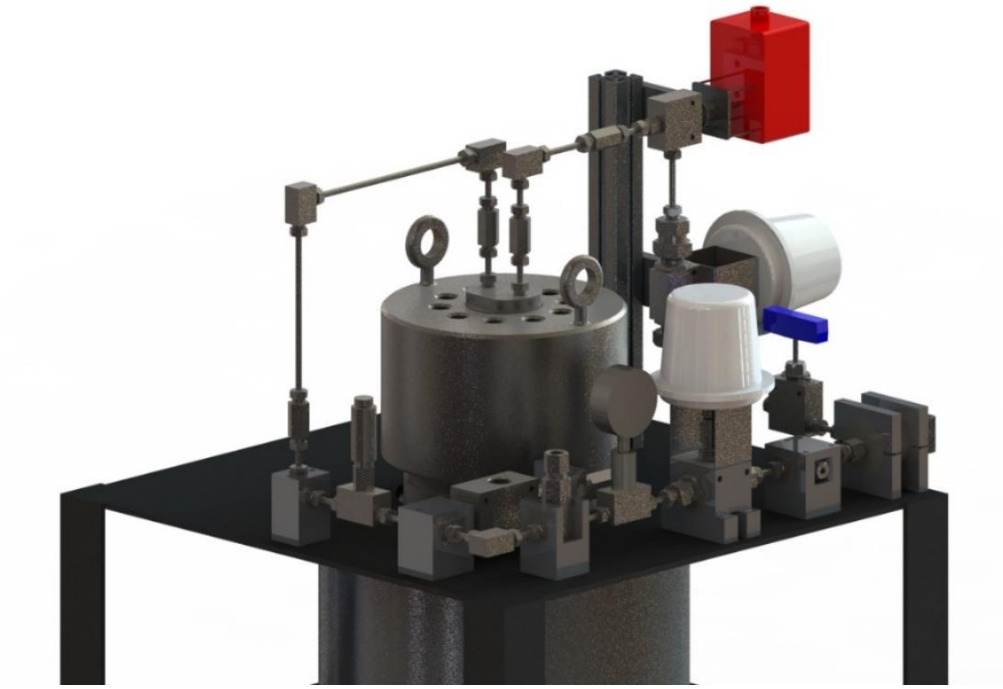

Figure 21: Final Rendering 1

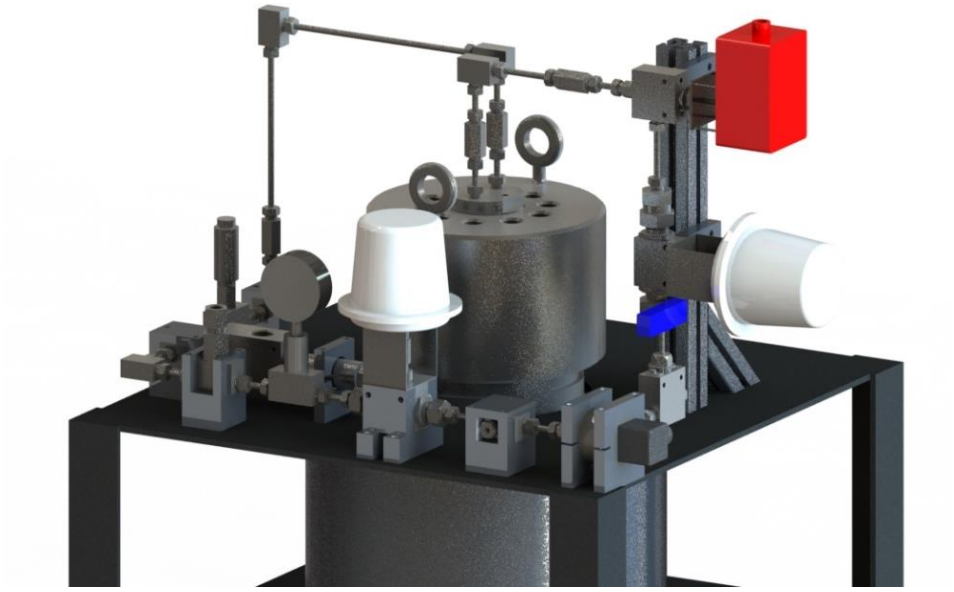

Figure 22: Final Rendering 2

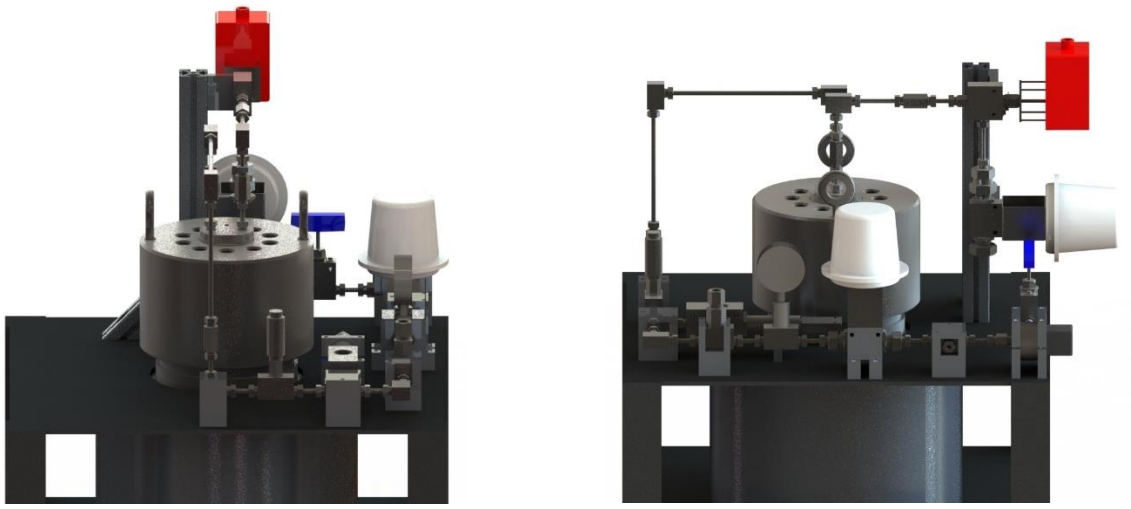

Figure 23: Final Rendering Front and Right Sides

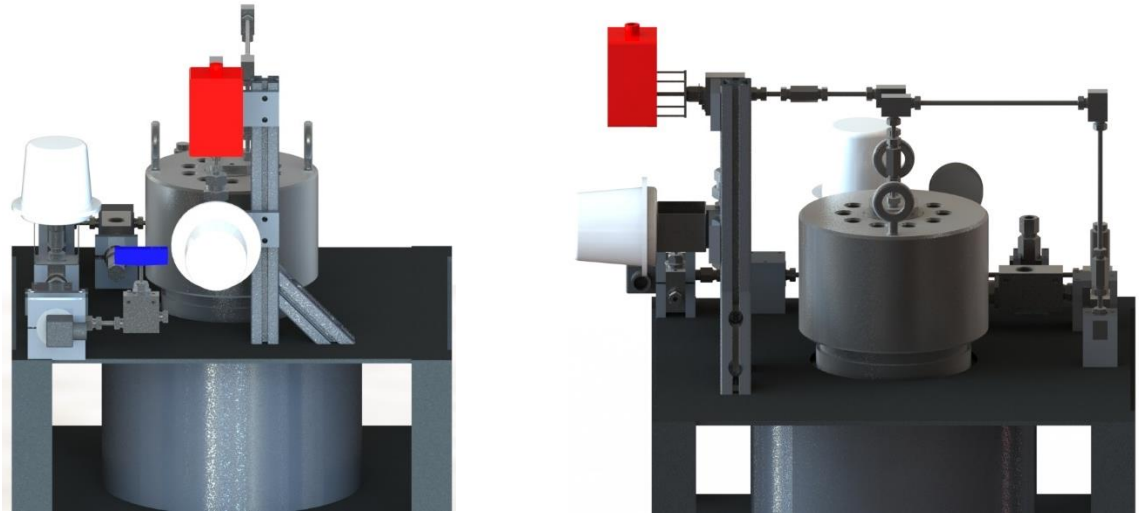

Figure 24: Final Renderings: Back and Left Sides

Figures 21–24 show CAD renderings of the manifold systems. These renderings follow the designs shown earlier in the section, but incorporate the machined mounts while providing a 3D view of the system in its completed form. Most notable is the alignment of the manifolds to the cart and pressure vessel. Furthermore, the completion of these renderings provided a basis for planning wire routing, manifold assembly procedures, and basic vessel assembly instructions. The next steps in the design process involved specifying support equipment, fully developing the electronics layout, and building a software program to run the device.

3.6 SUPPORTING EQUIPMENT

An important design goal was keeping the system as self-contained as possible. However, much supporting equipment is still required for operation. These components include a gas bottle connection manifold, bottle fill/bleed manifold, gas booster on/off valve, and flex lines.

At the recommendation of the gas booster supplier, three nitrogen gas supply bottles are used for filling the system. To connect the three bottles, a single row bottle manifold was acquired from Airgas® (Radnor Township, PA, USA). The manifold utilizes brass tubing and fittings, with flex lines coupled to the bottles themselves. There are on/off valves for each bottle as well as the entire manifold. To remotely control gas flow, solenoid valves are mounted to the outlet end of the manifold, one to control gas flow and the other to bleed the fill line to the atmosphere.

The gas booster is located on the floor next to the system. Supply drive air is run to the gas booster and controlled with a solenoid valve. High pressure flex lines, obtained from Spir-Star Ltd. (Houston, TX, USA), are run from the bottle manifold outlet to the gas booster inlet, and from the gas booster outlet to the system inlet tee.

3.7 ELECTRONICS

Requirements for the electrical design included 120V wall outlet operation, data acquisition (DAQ) device controller, and software control via LabVIEW (National Instruments, Austin, TX, USA). The electronics were broken down by required voltage and control requirements, then organized into individual circuits. After outlining all component electrical requirements, a data acquisition device and modules were chosen and programmed with LabVIEW.

The system components are organized into those that require 120V AC power and those requiring 24VDC power. While the AC components draw power directly from the wall outlet, the DC components are powered via DC power supplies. The total amperage requirements were calculated, and adequate power supplies were sourced. All high amperage components are controlled with solid state relays. The system was designed such that the current draw does not exceed 20 A while running at full capacity.

A National Instruments cRio 9030 was chosen as the onboard controller. Many factors contributed to this decision, such as the ability for embedded control utilizing the

onboard RT processor and field-programmable gate array (FPGA), four DAQ module slots, an onboard user interface, and ability for the cRIO to run downloaded programs without the need for a connected computer. Modules were chosen based on the component control requirements. These include a 9263 analog output module, a 9215 analog input module, a 9485 relay control module, and a 9211 thermocouple input module. A listing of electrical component requirements and power flow can be found in Appendix C.

3.7 Final Assembly

Final assembly consisted of machining the component mounts, assembling the high-pressure fittings, and wiring the system. Minor changes were made to the original design to better fit components to the cart. These changes included switching the inlet side bleed solenoid valve and needle valve, due to the availability of a 90° turn needle valve. Additionally, the exhaust side manifold was rotated in order to fit the components better. Pictures of the completed system can be found in Figures 25 through 28 below.

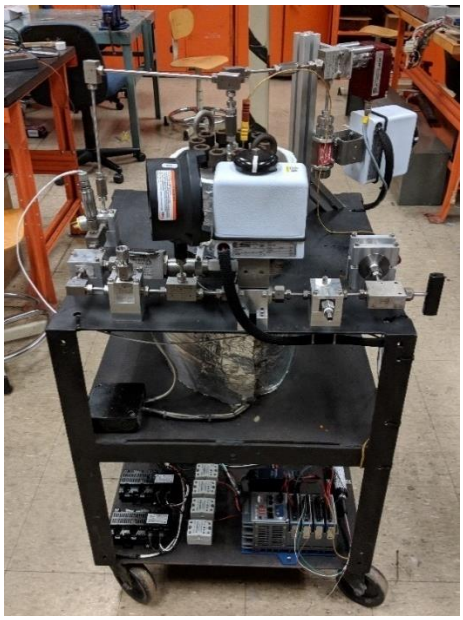

Figure 25: Assembled Device Right and Front Side

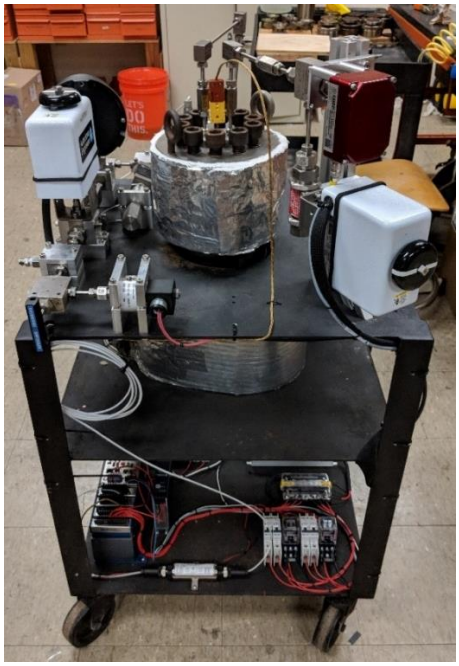

Figure 26: Assembled Device Back and Depressurization Manifold

Figure 27: Assembled Device Electronics View 1

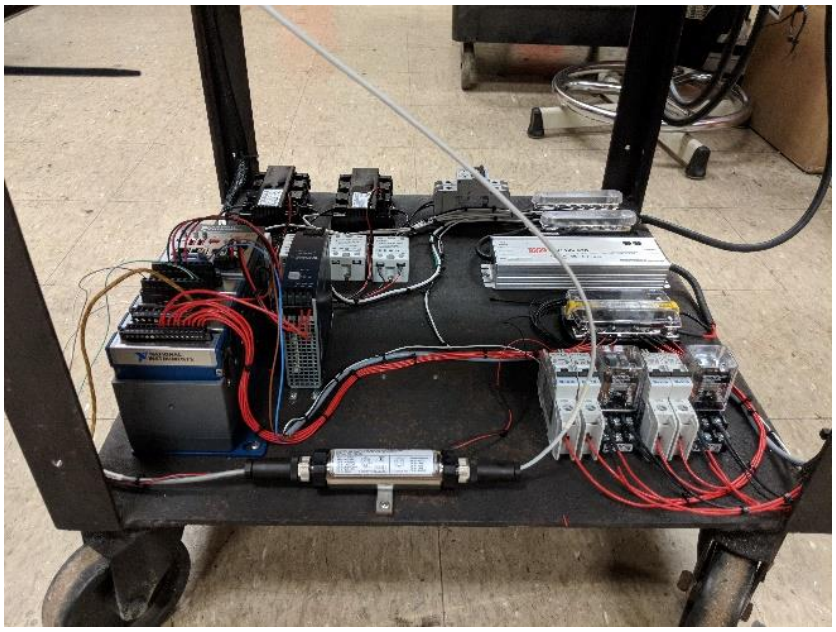

Figure 28: Assembled Device Electronis View 2

3.8 CONTROLS

Each component was checked individually for functionality with a base level I/O software before development of the control program began. The program is required to run continuously while monitoring test parameters, triggering valve actuation, and controlling depressurization rates. LabVIEW was used as the programming language, and a VI was built directly on the cRIO using the NI Real Time programming module.

Developing the VI was a step-by-step process. All system basic functions were incorporated into a continuously running `while` loop on the block diagram. Valve actuation was added by applying Boolean control on the front panel to each switch in the relay cRIO module. Test parameters such as pressure and temperature are displayed on the front panel by accessing data from their cRIO module channels. The metering valve actuator position was selected with a numeric control on the front panel. A safe guard was added to ensure control voltage provided to the metering valve actuator does not exceed its 1-5V range. Two parallel running loops were added to the block diagram, one to provide a running average of pressure values and another to control the heating bands based on gas temperature.

Depressurization rate control is based on an open loop design where the metering valve opening is dependent on a pressure range. For each pressure range there is a calibrated metering valve actuator output voltage. To accomplish this, a LabVIEW built-in case structure control is utilized. The control structure uses an integer as the case selector and pressure values as the means of advancing to the next case. For each case, a voltage

value, associated with a numeric control on the front panel, is output to the metering valve actuator while pressure is continuously monitored. When pressure falls below the specified range, the integer is increased by one, advancing the control structure to the next case.

While this method provides precise control over metering valve output, it does have some drawbacks. An open loop controller is not adaptive for differing test situations. The depressurization rate must be manually calibrated in each pressure region to a specific valve output. This process can be time consuming, but in situations where the test parameters do not change between tests, the same calibration can be used continuously. Furthermore, calibration values can be saved and accessed later to speed up the calibration process when changing to a new depressurization rate. A program flow chart is shown in Figure 29, and screenshots of the front panel and block diagram can be found in Appendix C.

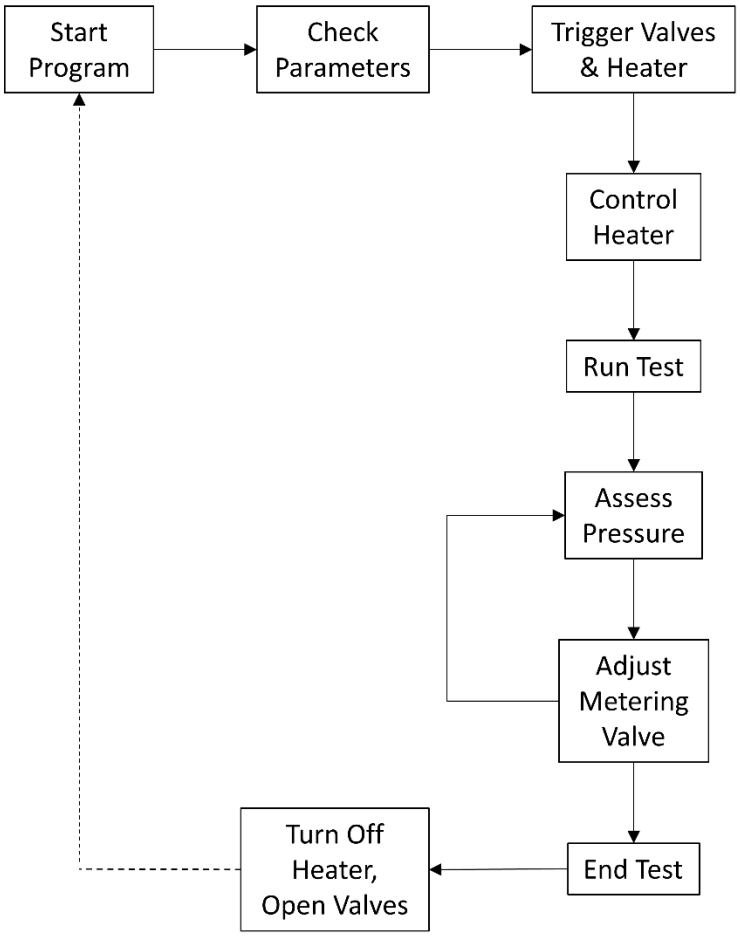

Figure 29: LabVIEW VI Program Flow Chart

4. TEST METHODS AND RESULTS

In order to examine the performance of the rapid gas decompression experiment device, a series of tests were prepared. Tests were based on the specifications found in NORSOK M710 and adapted to this test device. The polymers tested were those commonly found in oil well production use. The polymers were tested under varying temperatures and compressions. After testing, the polymer samples were sectioned and assessed for RGD damage. This chapter provides a complete report of the test findings.

4.1 TESTING PROCEDURE

A testing procedure was developed by following NORSOK M710 [19] guidelines and adapting them to the project sponsor testing requirements. The test preparation process involved defining important test parameters as well as developing a written test plan to follow while setting up and running the tests. The main testing parameters were pressure, temperature, dwell time, depressurization rate, and test medium. The pressure, dwell time, depressurization rate, and test media were held constant for all tests, while temperature was varied between tests. Since all but one test parameter was held constant, comparisons in damage were made by differing the test sample compound, size, durometer, and constraint method. The test parameters are discussed in detail below.

4.1.1 PARAMETERS

The test pressure was chosen as the maximum working pressure of the experimental setup, 10,000 psi. This working pressure satisfies NORSOK's requirement to test seals at their working pressure, as well as confirming the test device can operate at all pressures required by the sponsor.

M710 specifies "dry gas media [will] provide adequate indication of resistance to RGD" [19]. The main gas medium used in prior RGD testing was pure nitrogen, or a 90% nitrogen 10% carbon dioxide mixture. CO_2 requires special exhaust procedures to ensure safety in the test environment. Per sponsor requirements and to simplify testing procedure 99.9% pure N_2 was chosen as the test medium.

Test temperature was to be alternated between room temperature and the maximum rated working temperature for the test samples. For the samples chosen maximum working temperature is 250°F. Tests were alternated between 75°F and 250°F.

NORSOK M710 specifies a depressurization rate of 1000 psi/min [19]. M710 also states that, "a non-standard decompression rate shall be specified if required by service application conditions" [19]. Using this notion and recommendations from the sponsor, a slower rate of 300 psi/min was specified. This rate was held constant from an initial pressure of 10,000 psi to the final pressure of 0 psi gauge.

The dwell time was chosen to ensure full gas diffusion into the elastomers, but also to reflect the exposure period found in the application environment. Per sponsor recommendation, both these requirements are satisfied with a 24-hour dwell period.

4.1.2 TEST SAMPLES

Test sample elastomers were chosen to reflect those used in oil and gas RGD applications, such as FKM, HNBR, Aflas®, and Nitrile [31]. Readily available compounds of Buna-N and Viton were obtained from McMaster-Carr®; Buna-N is another name for Nitrile rubber and Viton most closely resembles Aflas®. Elastomer samples are available in several types of geometries, including molded rectangular strips, cylindrical pucks, flat sheets, and O-rings. O-rings provide the best option for varying thickness as well as providing compression to the samples via a piston seal fixture.

O-ring sizes -223 and -312 were chosen. A -223 size O-ring has a 1/8" cross section with a 1 7/8" outer diameter and 1 5/8" inner diameter. A -312 size O-ring has a 3/16" cross section with a 1" outer diameter and 5/8" inner diameter. Buna-N O-rings were sourced in 70 and 90 durometers and Viton O-rings were sourced in 75 and 90 durometers.

Both sizes of O-ring were tested in unconstrained and constrained configurations. The unconstrained O-ring provides information on RGD damage caused purely by the stress state imposed from gas diffused in the elastomer. Constraining the O-ring provides a method of viewing RGD damage to the elastomer in its actual application environment. The constraint provides additional stress states within the elastomer due to the compression imposed in the O-ring gland. Fixtures were provided by the sponsor to constrain both sizes of O-ring; esign drawings of the fixtures are available in Appendix D. The fixtures comprise four pieces: an inner piston, an outer cylinder, and top and bottom caps. Constraint, in the form of O-ring squeeze, was imposed by the piston's outer gland

diameter and the cylinder's inner diameter. The O-ring is allowed to expand laterally in the O-ring groove. The width of the groove is determined by the distance between the piston shoulder and the cap shoulder. A final squeeze can be calculated by using equation (4), where *S* is the squeeze percentage, B_d is the bore diameter, G_d is the gland diameter, and *CS* is the O-ring cross section [32]:

$$S = 1 - \frac{(\frac{B_d - G_c}{2})}{CS} \quad (4)\backslash$$

Applying equation (4) to both sizes of O-rings, based on their fixtures, results in a squeeze of 20.50% for the -223 size and 18.80% for the -312 size.

4.1.3 Design of Experiments

Combining the test parameters of pressure, temperature, depressurization rate, and dwell time, along with sample compound, durometer, size, and compression, a full design of experiments (DOE) table was created. The DOE consists of 32 combinations of test samples subjected to four separate tests, while pressure and depressurization rate are held constant. Table 4 below shows the variation between test samples, while the full DOE can be found in Appendix E.

Compound	Durometers	Widths	Size	Squeeze in Fixture	Test Temperatures
Buna-N	70	1/8"	-223	20.50%	75
	90	3/16"	-312	18.80%	250
Viton	75	1/8"	-223	20.50%	75
	90	3/16"	-312	18.80%	250

Table 3: Variation of Test Samples

4.1.4 TEST PROCEDURE

Before testing began, a test procedure check list was developed. The procedure involves inserting samples, reassembling the device, setting up the LabVIEW VI, starting the heaters, charging the device with gas, starting the depressurization process, and disassembling the device to remove samples. A written test procedure is critical in ensuring operator and building safety during test operation. The full test procedure can be found in Appendix D.

4.2 TEST RESULTS

After concluding the four tests, all aspects of the test device's operation were compared to the design goals. The device is capable of pressurizing to 10 ksi in under an hour, which exceeds the calculated time for pressurization. The device can heat the pressure vessel to 250°F within four hours and maintain temperature during the test dwell time. The device can be operated fully from a computer located in a safe location away from the device (including in another room). The relief valve is confirmed to bleed pressure from

the system above 10,250 psi, rendering a possible over-pressure situation unlikely. After calibration, the system is capable of depressurizing in a linear manner, in this case 300 psi/min. Figure 30 shows the depressurization curve for one test carried out in this research. Other depressurization curves are available in Appendix E.

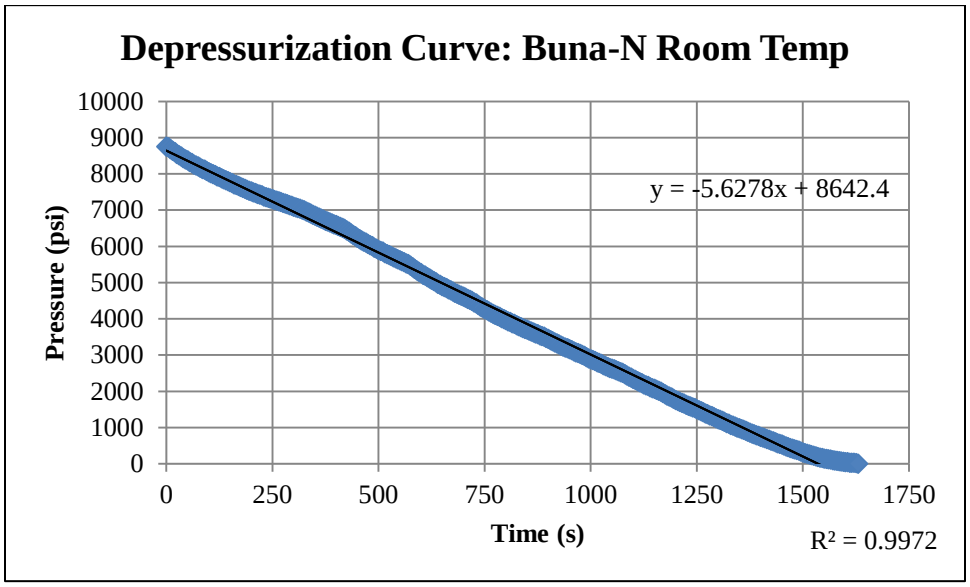

Figure 30: Depressurization Curve: Viton Room Temperature Test

The test device met all design goals with a few exceptions. The first problem encountered was a loss in pressure during the 24 hour dwell time. The pressure loss average between the four tests was roughly 1,000 psi. Second, the calibration process to obtain a linear depressurization curve using open loop control of the metering valve is a time-consuming process. Third, and finally, the predicted depressurization rates for the VRMM metering valve were lower than found during testing. The system is capable of depressurizing well above 1,000 psi/min but cannot obtain a linear depressurization curve

below 250 psi/min for the entire pressure range. For the tests carried out in this research these issues were not a large concern. However, steps are being taken to eliminate these problems during future use and will be proposed in section 4.4.

After finishing the testing process, the samples were sectioned and analyzed for RGD damage. The samples were given a damage rating in accordance to the guidelines in M710. First the samples were inspected for external RGD damage. Then, the samples were cut into four pieces, as shown in Figure 31. Each cut was examined for cracking and bubbles, then given a 0 – 6 rating for observed damaged based on Table 1 (see section 2.3). The ratings for each sample were then added to create a total damage tally for each sample. Using this data, correlations were made between the different combinations of sample compound, durometer, constraint, and test temperature. The results can be found in the completed DOE found in Appendix E. The following section provides pictures of RGD damaged in selected samples as well as the correlations made, summarization of results from the DOE, and explanation of the damage phenomena in relation to the background information presented in Chapter 2.

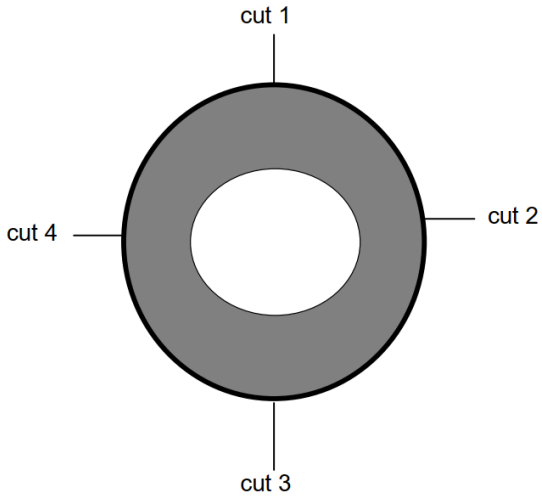

Figure 31: O-ring Sectioning Guideline [19]

4.3 Analysis of Elastomer Samples

Inspection of the sectioned samples resulted in finding significant damage in over half of the 32 tested O-rings. The Viton samples in the 250°F test suffered the worst damage. Buna-n at 250°F also suffered substantial damage. Both compounds at room temperature show very little to no damage at all. In this section samples are compared between their test parameters, damage is analyzed and compared to the damage types proposed in the background section, and general assessments are proposed on how temperature and constraint method affects the level of RGD damage.

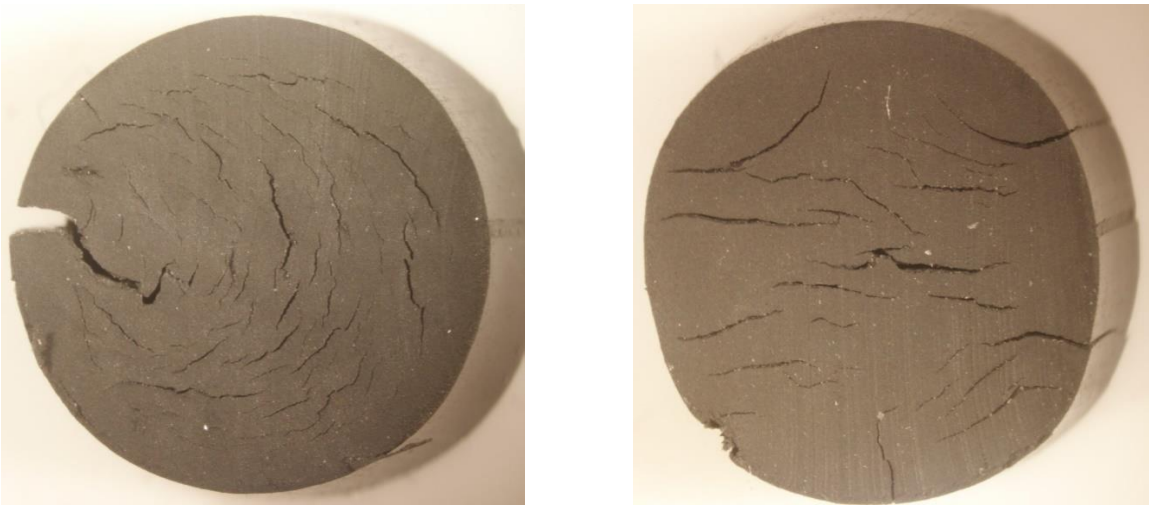

Figure 32: Damage in -312 Viton 75 at 250°F; Left is Unconstrained, Right is Constrained

Figure 32 shows -312 Viton 75 O-ring samples tested at 250°F. It is easy to see both samples are heavily damaged, with the unconstrained sample on the left rated at level 5 damage, and the constrained sample rated at level 4 on the 1-6 damage scale provided by M710. The clear differences between the two samples are damage type and orientation. Both samples are oriented horizontally, with the outer diameter to the left and inner to the right. The unconstrained sample has cracking in a radial direction, extending from the center axis of the cross-section, and a rupture to the exterior surface on the outer diameter of the seal. The constrained sample has predominately horizontal cracking throughout the entire cross-section. One explanation of the difference in damage types is that the unconstrained sample follows the methodology proposed in [15], where radial cracking is a result of the non-uniform stress state within the O-ring caused by shear stress gradients generated between the outer and inner regions due to a pressure differential. The sample

on the right in the figure is constrained in the same manner as in [16]. Briscoe and Liatsis hypothesize that the elastomer ruptures due to hydrostatic tension, but localized stress fields control the direction and location of cracking. In the present case, the method of constraint compresses the seal in the horizontal direction, causing cracks to propagate in the horizontal direction.

Figure 33 shows a -312 Viton 90 O-ring tested at 250°F and constrained. This sample shows very severe RGD damage rated at level 5, possibly level 6, on the M710 scale. The top crack extends from the outer diameter of the O-ring, nearly all the way to the inner diameter, separating the seal into two different fragments. Damage such as this renders the seal completely useless in its application environment, possibly causing significant downtime in the application operation environment, or complete failure.

Figure 33: Severe RGD Damage; -312 Viton 90, 250°F, Constrained

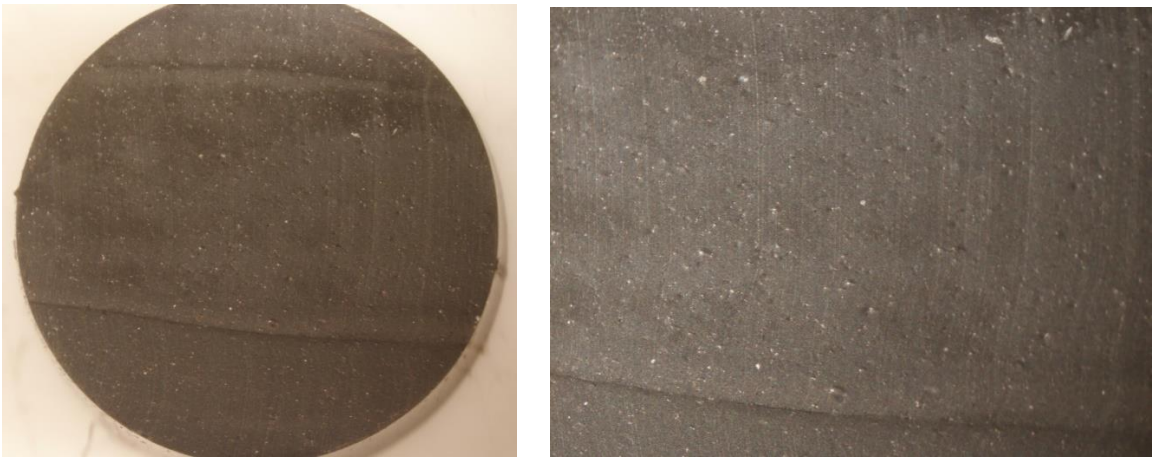

Figure 34: Bubbling in -312 Buna-N 70 at 75°F, Unconstrained

An interesting phenomenon can be seen in Figure 34, where the Buna-N O-ring samples run at 75°F show an onset of RGD damage in the form of small bubbles throughout the sample cross section. These samples are better seen in the zoomed picture of the cross section on the right of Figure 34. While the samples did not suffer from any cracking, the bubbles found are an indication of gas permeation into the elastomer. This is an indication that even at room temperature, RGD damage can be an issue for elastomers under long exposure to gases at elevated pressure.

Multiple types of RGD damage and possible explanations for their occurrence are proposed in this section. By examining the complete DOE, available in Appendix E, it is also possible to propose some general explanations of the effects of individual test parameters. First, there appears to be a correlation between temperature and the level of damage. Samples from tests run at 75°F showed no damage or small bubbling, with no

cracks, while the samples from tests run at 250°F all showed very significant cracking. One explanation of this correlation is that increased gas diffusion in elastomers at high temperature causes increased damage. The experimental data also show that high durometer elastomers are more resistant to RGD damage than lower durometer compounds. In both tests run with Buna-N, the high durometer samples suffered less damage than the low durometer samples. The Viton samples suffered roughly the same amount of damage regardless of durometer. Finally, compressing the elastomer sample reduces damage to the sample. This correlation is evident in all tests, regardless of compound, durometer, constraint, and temperature.

The main purpose of the experiments in this research was to evaluate the performance of the test device, which will be discussed in the next section. The testing also provided an opportunity to observe trends in seal performance and to propose possible explanations for the behaviors observed. Only a limited number of tests were conducted. Additional testing is required across a larger range of test parameters and compounds to propose recommendations on minimizing RGD damage in application environments.

5. CONCLUSION AND RECCOMENDATIONS

5.1 SUMMARY OF EQUIPMENT CONSTRUCTION

The goal of this research was to develop a high-pressure device for testing RGD damage resistance of elastomers. The design goals for the system included a working pressure of 10 ksi, test temperature up to 400°F, linearly controlled depressurization rates of 5–1,000 psi/min, and remote operation. Using a pressure vessel and cart provided by the project sponsor, the device was designed and constructed. The design process involved developing initial concepts of the redesigned system, specifying components necessary for system operation, developing a final design in CAD software, creating manifold attachment apparatuses, assembling the system, wiring the electrical components, and developing software to operate the system. Upon completion of the system, experimentation was conducted on elastomer samples to evaluate device performance.

5.2 RESULTS AND TESTING CONCLUSIONS

High-pressure testing of elastomer O-ring samples was used to evaluate device performance, as well as to develop an understanding of RGD damage with respect to damage theories summarized in Chapter 2. In over half the tests RGD damage was observed in the test samples. Furthermore, damage in the samples reflected the two types of possible damage proposed, radial cracking due to a pressure difference in the O-ring cross section and parallel cracking due to stresses imposed by the seal constraint method.

Beyond comparing theoretical damage to that observed, qualitative correlations were proposed that relate RGD damage in the samples to test temperature, sample durometer, and constraint method. While the knowledge gained on RGD during the tests was beneficial, more importantly, the test device was confirmed to meet its design goals. Tests were carried out at 10 ksi, 250°F, and use of an actuated micrometering valve allowed depressurizing in a linear manner at 300 psi/min across the entire pressure range. The shortcomings of the device were identified as a 10% pressure loss, need for lower depressurization rates, and lengthy calibration procedure. Solutions for these problems are presented below. At the conclusion of this report, the test device will be presented to the project sponsor as operational and further testing to their requirements can be carried out.

5.3 TEST DEVICE IMPROVEMENTS

The main goal of this research to was design and build a test device to evaluate the effects of RGD damage on elastomers. Overall, the system appears to have achieved this goal. However, there are three major concerns that should be addressed to improve the system: eliminating pressure loss during dwell time, achieving lower depressurization rates, and minimizing test calibration time.

The 10%-15% pressure loss over a 24-hour dwell time is a major concern to future testing with the system. This pressure leak might occur in several locations between the ball valves in the two manifolds and the pressure vessel. However, all components in the manifolds are off-the-shelf Autoclave brand components that were assembled according to

a strict procedure outlined by the manufacturer. It was discovered during testing that the provided pressure vessel was modified by the previous owner. The interior of the vessel was machined and re-cast with a Hastelloy material for acidizing tests, and the cap was re-machined to accommodate an Autoclave Speed-Bite connection for the thermocouple adapter. Along with these modifications, the sealing gland was machined to previous owner's specifications and no longer uses an off-the-shelf pressure vessel sealing ring available from HIP. While the pressure vessel was obtained with a hydrostatic pressure test certification, the vessel customization can be a main contributor to pressure loss over the dwell period. One way to locate the leak is to pressurize the system with helium and use a helium detection device and spot sniffer to find all sources of gas leaks. Possible solutions for the theorized leaks are to re-machine the vessel and cap sealing groove to better accept a standard size O-ring and have a proper surface finish for sealing. The thermocouple gland can also be re-machined to accept an appropriate HIP high pressure thermocouple well like the one that originally came with the vessel. Pressure loss should be the first problem addressed.

Lowering the depressurization rates must be solved by adding additional hardware to the system. The rates achieved in this report were already a result of adjusting the MCL actuator settings to decrease the VRMM valve opening to a maximum of one turn, as well as increasing actuator torque to fully close the metering valve. One solution to this problem is to add a secondary depressurization metering valve. This can be accomplished by adding a tee to the inlet manifold, followed by an actuated on/off needle valve, and a very fine

micrometering valve. This solution is being implemented at the time of submission of this thesis.

The final proposed improvement is to develop a closed loop depressurization control program. The current method of depressurization utilizes user tuned open loop control values for 500 psi pressure ranges. This method requires a considerable amount of time to calibrate the system prior to running tests, with the advantage of completely identical depressurization rates between tests. It would be beneficial to build a closed loop program that reads pressure differential over time as an input and adjusts the metering valve accordingly to obtain the desired rate. This system upgrade is also a work in progress.

APPENDICIES

APPENDIX A: EQUIPMENT DRAWINGS

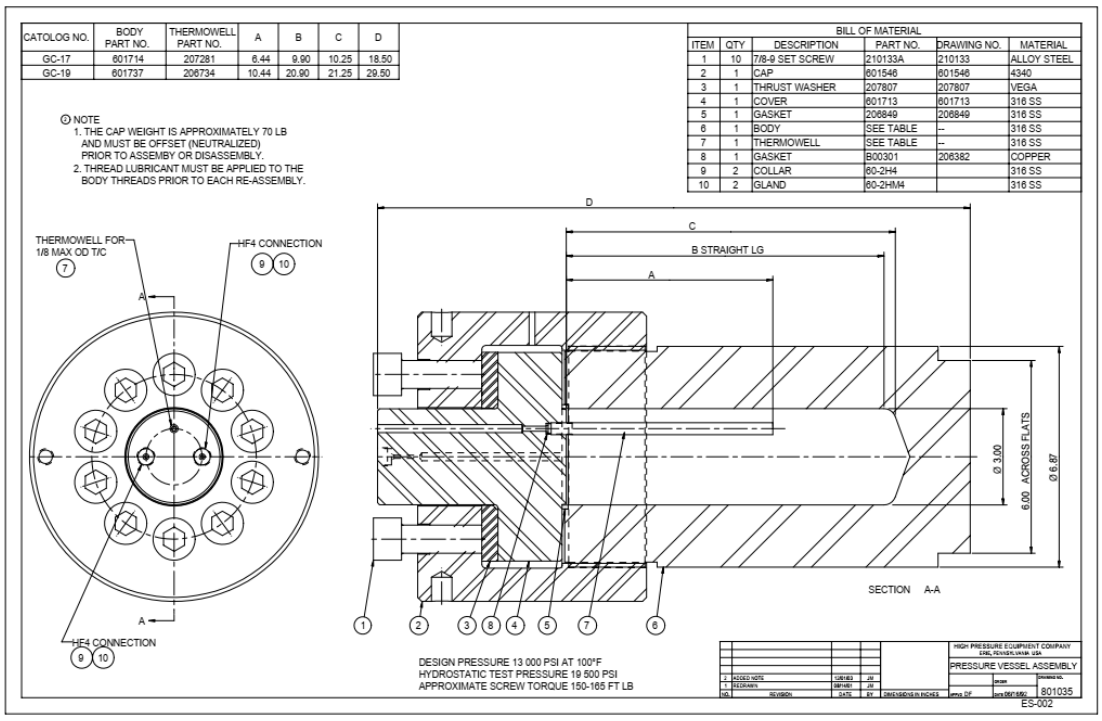

Figure 35: Pressure Vessel Design Drawing

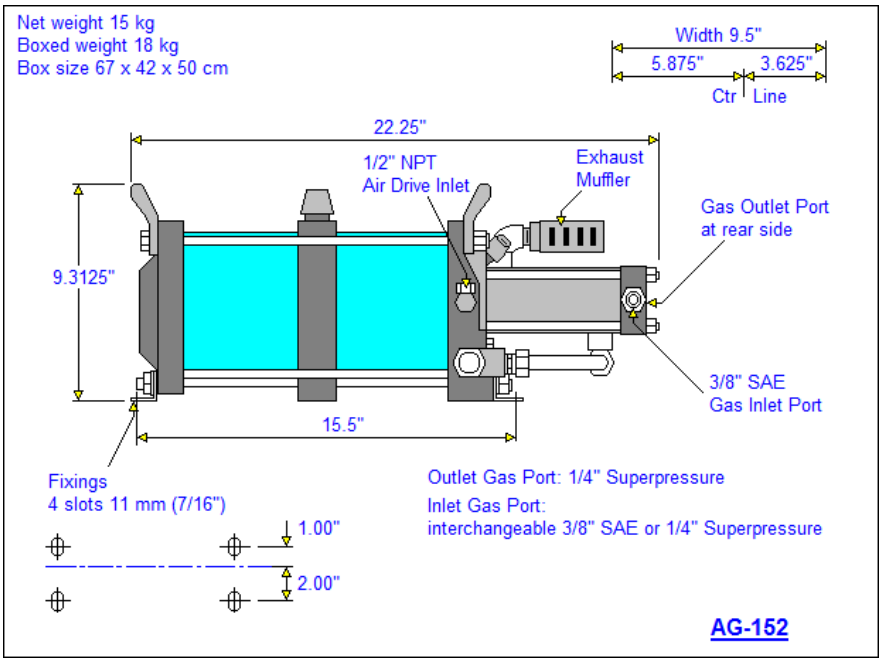

Figure 36: High Pressure Gas Booster Drawing

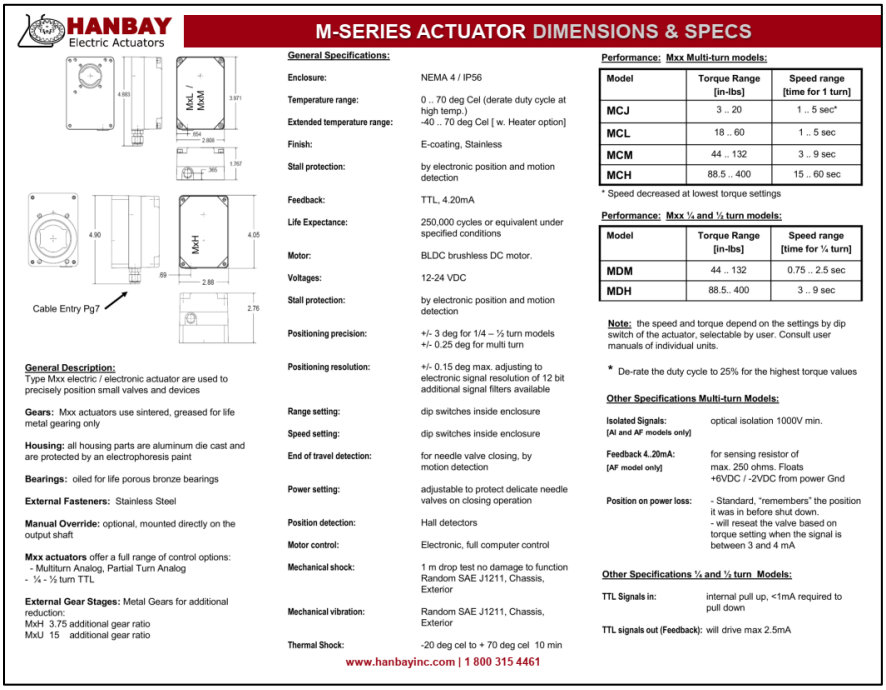

Figure 37: Hanbay MCL Actuator Drawing

APPENDIX B: BILL OF MATERIALS

Manufacturer	Part	Part Number	Quantity	Price per	Total Price
Autoclave					
	Micro Metering Valve	30VRMM4812 – TG	1	$410.00	$410.00
	Relief Valve	15RVP9072 – HT	1	$1,843.00	$1,843.00
	Safety Head	CS4600 - 3/16F	1	$96.89	$ 96.89
	Burst Disk	P-7060	1	$67.05	$67.05
	Exhaust Ball Valve and Actuator	2B4S20H9 - HT - E03	1	$1,545.00	$1,545.00
	Inlet Ball Valve and Actuator	2B4S20H4 - HT - E03	1	$1,494.00	$1,494.00
	M/F Adapter (for BV) 1/4 to 9/16	60M94B3	1	$58.58	$58.58
	PV Adapter HP to JIC	20MFAH4J4	1	$50.60	$50.60
	Coupling	60F4433	4	$81.85	$327.40
	1/4" Elbow HP	CL4400	4	$83.71	$334.84
	1/4" Tee HP	CT4440	4	$132.00	$528.00
	2.75" Nipple	CN4402-316	16	$17.65	$282.40
	High Anti-Vibration Collet Gland	KCGL40-316	4	$21.90	$87.60
	4" Nipple	CN4404-316	2	$23.44	$46.88
	8" Nipple	CN4408-316	1	$30.98	$30.98
	10" Nipple	CN44010-317	1	$33.35	$33.35
	12" Nipple	CN44012-316	1	$34.60	$34.60
	NPT Adapter (M 1/4NPT; F F250C)	15M44N3	2	$35.20	$70.40
	M to M adapter (RV)	20MAM9H4	1	$52.67	$52.67

Hanbay					
	Metering Valve Actuator	MCL-050AB-1-10VRMM4812	1	$1,481	$1,481
Omega					
	Pressure Transducer and Amplifier	SYS/PX1004L1-10KAV/IN-UVI-CAL3	1	$2,798	$2,798
	High Pressure Solenoid Valve	SVH-111	1	$580	$580
Haskel					
	Gas Booster	2881-AG-152-C	1	$5,180	$5,180
National Instruments					
	cRIO-9030 Module	783450-01	1	2,888.10	2,889.10
	NI-9263 Analog Output Module	779012-01	1	$410	$410
	NI-9215 Analog Input Module	779011-01	1	$542	$542
	NI-9211 TC Input Module	779001-01	1	$356	$356
	NI-9485 Relay Module	779600-01	1	$345	$345
	PS-15 24 VDC Power supply	781093-01	1	$215	$215
	Panel Mount Kit for CRIO	157253-01	1	$59	$59
	Panel Mount Kit for Power Supply	199432-01	1	$31	$31
McMaster Carr					
	Hybrid Long-Life Medium-Current Relays	8670K1	2	$52.93	$105.86

	DPDT 24VDC Relays	1358T14	2	34.93	$69.86
	Relay Sockets	1358T21	2	11.9	$23.80
	120AC Solid State Relay	7456K21	4	36.54	$146.16
	Gas Thermocouple	3856K83	1	23.37	$23.37
	Surface Thermocouple	3648K24	2	25.69	$51.38
	Thermocouple Connector RP Female	3869K55	1	14.3	$14.30
	Thermocouple Wire 10ft	3870K53	1	22	$22.00
	Solenoid Valve, Supply Air	4639K75	1	$98.38	$98.38
	High Pressure Solenoid Valve	1190N14	2	109.08	$218.16
	Power Dist Bar AC	9290T14	2	21.41	$42.82
	Power Dist Bar Cover AC	9290T21	2	4.58	$9.16
	Power Dist Bar DC	9290T11	1	$33.80	$33.80
	T-slot framing, Diagonal Brace 40mm	5537T201	2	$19.66	$39.32
	T-slot framing, single rail, 40mm, 2ft	5537T102	1	$19.93	$19.93
	T-slot Fasteners	5537T458	3	$5.05	$15.15
	T-slot 40mm end caps	5537T24	1	$1.73	$1.73
	Wire, 14 Gauge, Black, 25ft	8054T17	1	$11.27	$11.27
	Wire, 14 Gauge, White, 25ft	8054T17	1	$11.27	$11.27

	Wire, 16 Gauge, Black, 100ft	8054T16	1	$23.04	$23.04
	Wire, 16 Gauge, White, 50ft	8054T16	1	$12.67	$12.67
	Wire, 16 Gauge, Red, 50ft	8054T16	1	$12.67	$12.67
	Wire, 18 Gauge, Black, 25ft	8054T15	1	$5.03	$5.03
	Wire, 18 Gauge, Red, 25ft	8054T16	1	$5.03	$5.03
	Ring Terminals, #8, 100	7133K38	1	$7.74	$7.74
	Ring Terminals, #10, 100	7113K12	1	$9.28	$9.28
	Ring Terminals, 1/4", 100	7133K13	1	$12.07	$12.07
	Heat Shrink, 0.21" ID, 25ft	7864K32	1	$11.14	$11.14
	Heat Shrink, 0.4" ID, 25ft	7864K34	1	$15.78	$15.78
	Foil-faced insulation 0.5" 3"x12'	9379K93	1	$14.31	$14.31
	Foil-faced insulation 0.5" 2"x12'	9379K92	1	$12.46	$12.46
	Ceramic Insulation Roll, 1", 24"x25'	93315K34	1	$61.82	$61.82
	Cable tie assortment	7338K36	1	$13.14	$13.14
	Aluminum Foil Tape, 1", 5 Yards	7594A8	1	$17.86	$17.86
	DIN 3 Rail, 7.5mm, 1m	8961K15	1	$5.07	$5.07

	1/4"-20 x 4" socket head, 10 per	92196A558	2	$8.53	$17.06
	M6 x 100mm socket head, 5 per	91292A205	1	$4.60	$4.60
	1/4"-20 x 2" socket head, 25 per	92196A801	1	$11.17	$11.17
	1/4"-20 x 3" socket head, 10 per	92169A554	1	$5.60	$5.60
	5/16"-18 x 1-3/4" hex flathead, 10 per	92210A589	1	$4.99	$4.99
	Fiberglass sleeving, 1" ID, 5ft	8760T26	1	$18.67	$18.67
	Fiberglass sleeving, 3/4" ID, 5ft	8760T24	1	$14.65	$14.65
	Fiberglass sleeving, 1/2" ID, 5ft	8760T22	1	$10.93	$10.93
	Electrical Tape, 1", 5 yards	3468A12	1	$36.59	$36.59
Automation Direct					
	Circuit Breaker, 1.5A	FAZ-C1P5-1-NA-SP	2	$37.00	$74.00
	Circuit Breaker, 4A	FAZ-C4-1-NA-SP	1	$18.50	$18.50
	Solid state relay, 3-32 VDC input, 10A, 24-280 VAC load	AD-SSR610-DC-280A	4	$16.25	$65.00
	Circuit Breaker, 0.5A	FAZ-C0P5-1-NA-SP	1	$18.50	$18.50
	Circuit Breaker, 6A	FAZ-C6-1-NA-SP	1	$18.50	$18.50
	Circuit Breaker, 3A	FAZ-C3-1-NA-SP	1	$18.50	$18.50

TRC Electronics, INC.					
	24VDC Power Supply	HEP-185-24A	1	$75.20	$75.20
SPIR STAR					
	HT Hose Grey, 1/4-28 HP nipple ends, 6ft	made to order	1	$155.60	$155.60
	Hose Blue, 1/4-28 HP nipple ends, 10ft	made to order	1	$166.60	$166.60
Airgas					
	Manifold single row, model SRB 3	ADQSRB43580	1	$1,457.30	$1,457.30
	Valve Diaphram Stainless Steel 1/2" MNPT x FNPT	ADQSG6475N	1	$386.30	$386.30
				Total	$ 26,054.63

Table 4: Bill of Materials

APPENDIX C: CONTROL COMPONENTS AND DIAGRAMS

Component	Voltage	Amperage	Relay	Breaker	cRIO Control
Heating Band #1	120V AC	1.67	SPST High Amp	3 amp	AO
Heating Band #2	120V AC	4	SPST High Amp	6 amp	AO
HP Solenoid	120V AC	0.2*	Solid State	No	Swiching
cRio	24VDC	N/A	No	No	N/A
24VDC Power Supply	120V AC	7.8*	No	No	N/A
cRio Power Supply	120V AC	5*	No	No	N/A
Bottle SV	120V AC	1*	Solid State	No	Switching
Fill Bleed SV	120V AC	1*	Solid State	No	Switching
Gas Booster SV	120V AC	1*	Solid State	No	Switching
MV Actuator	24VDC	3*	No	4 amp	AO
Ball Valve Actuator #1	24VDC	1*	DPDT	1.5 amp	Switching
Ball Valve Actuator #2	24VDC	1*	DPDT	1.5 amp	Switching
Pressure Transducer	24VDC	0.2	No	0.5 amp	AI
K Thermocouple	N/A	N/A	No	No	TC
* Denotes Max Amperage Draw for Components not Under Full Time Use					
Legend					
SV = Solenoid Valve					
SPST = Single Pole Single Throw					
DPDT = Dual Pole Dual Throw					
AO = Analog Output NI 9263					
Switching = NI 9485					
AI = Analog Input NI 9215					
TC = Thermocouple NI 9211					

Table 5: Electrical Components

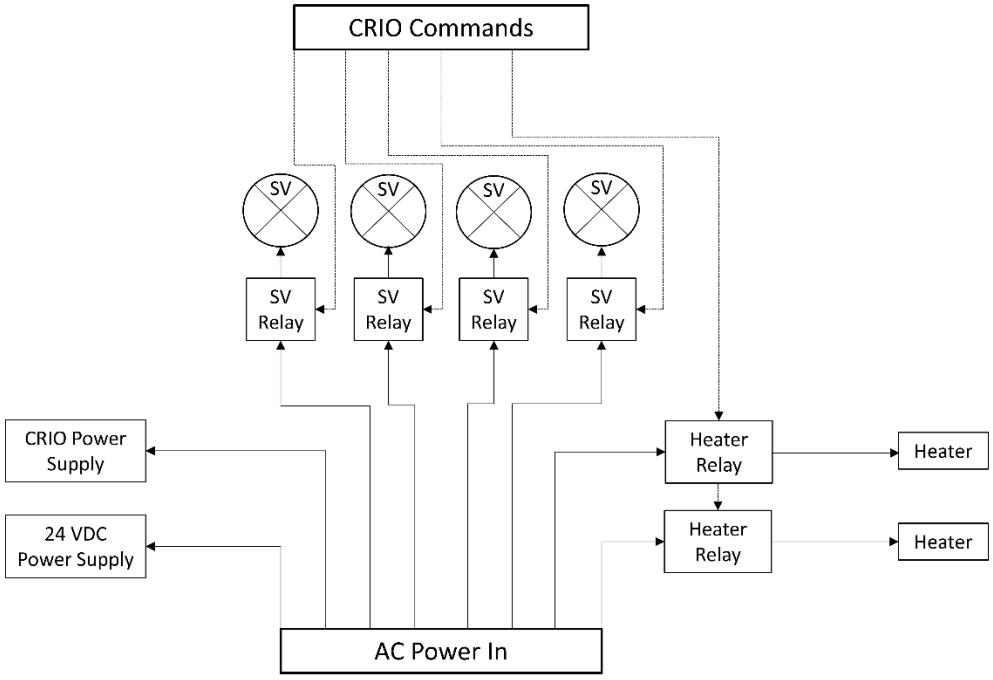

Figure 38: AC Power Flow Diagram

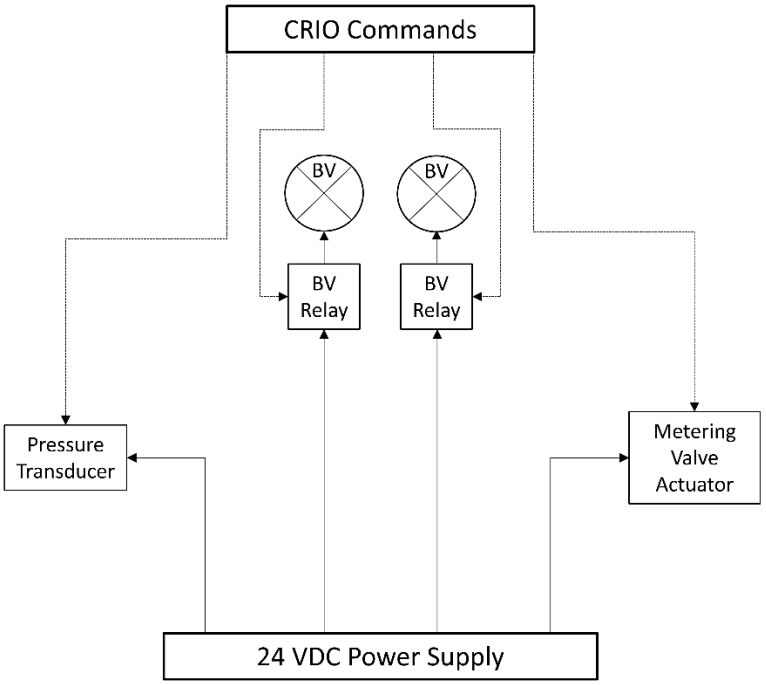

Figure 39: 24 VDC Power flow Diagram

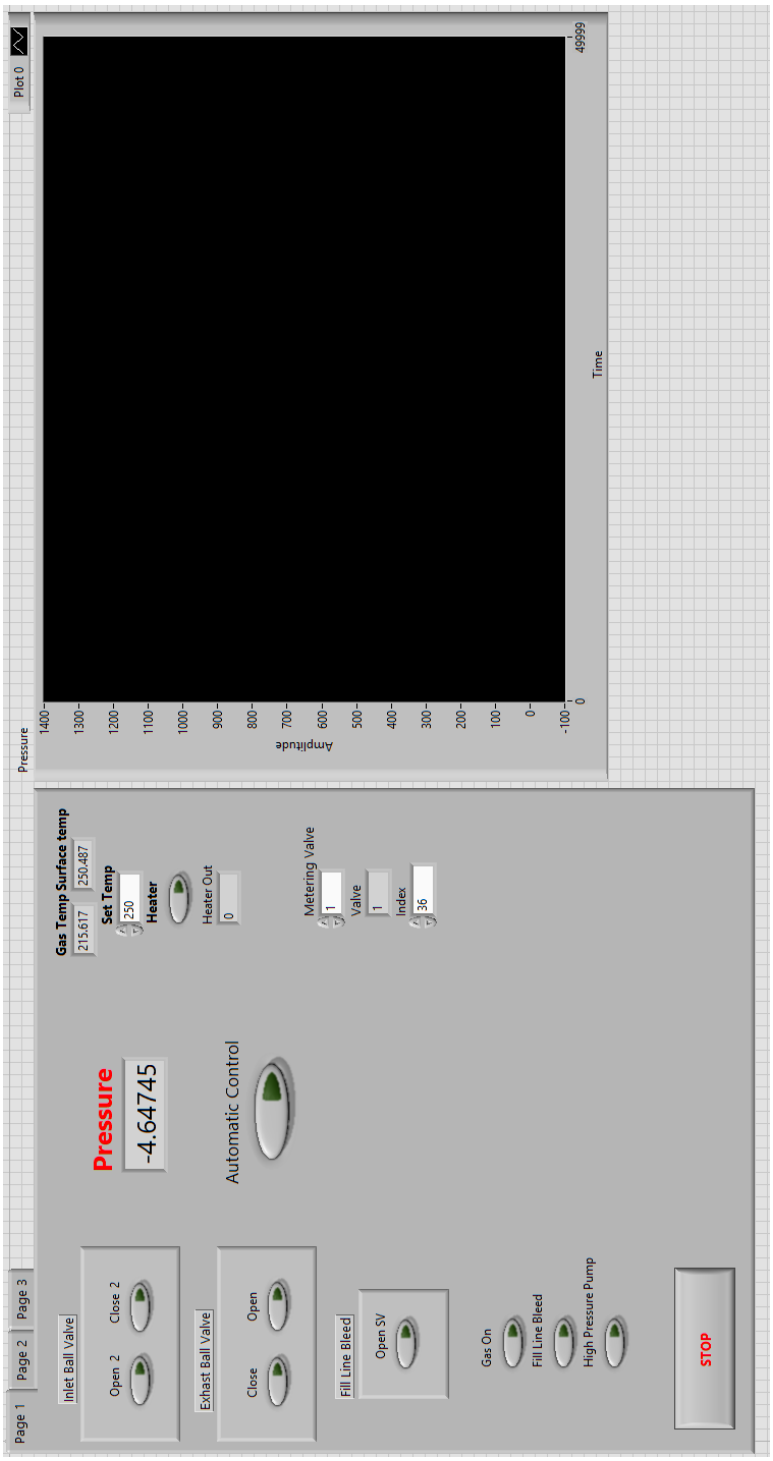

Figure 40: Control VI Front Panel

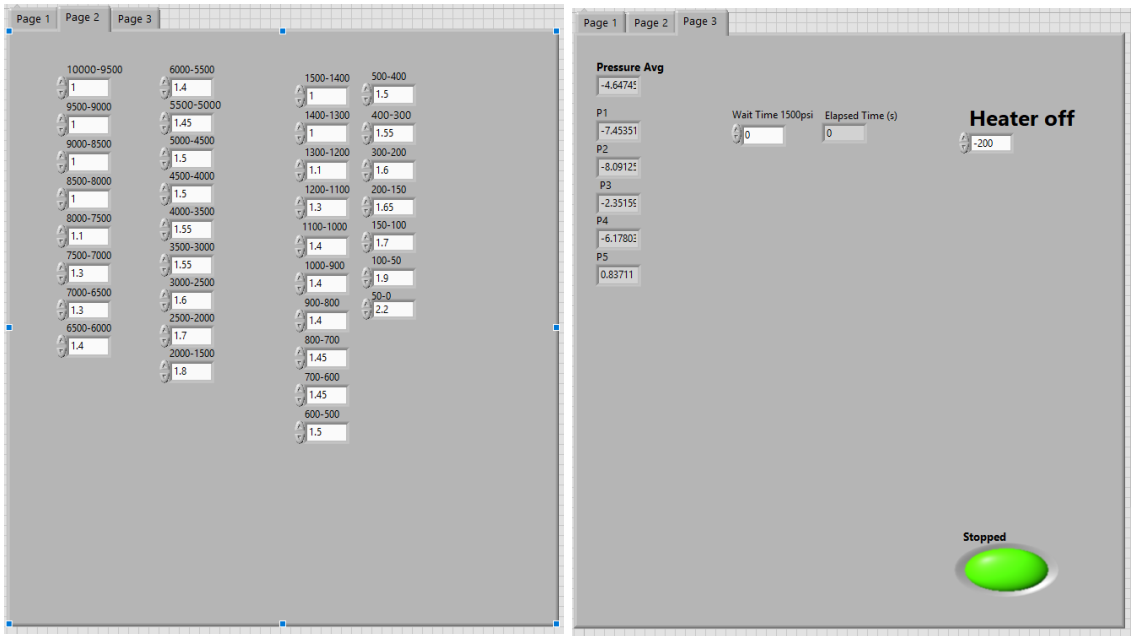

Figure 41: Control VI Front Panel: Pages 2 and 3

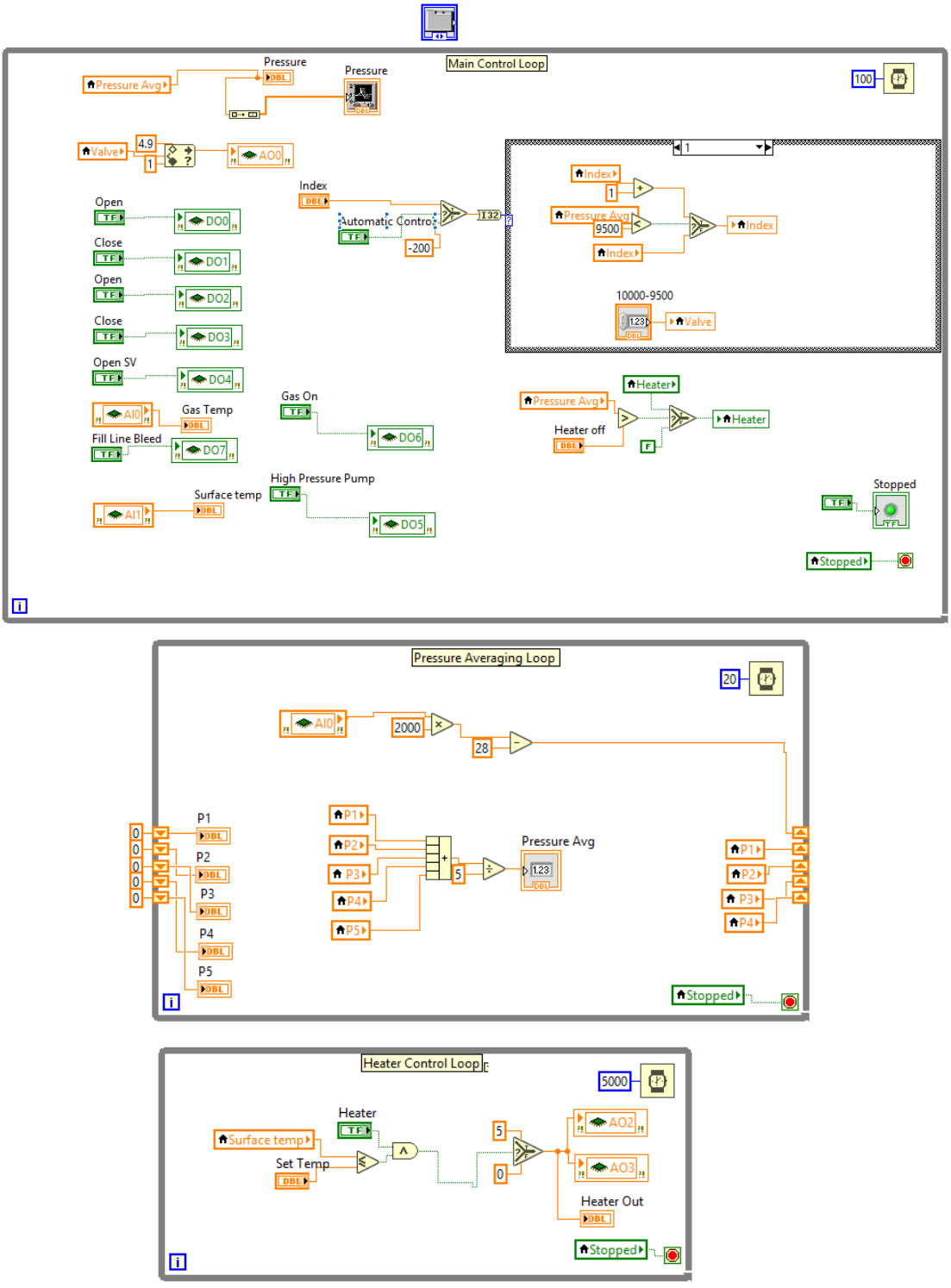

Figure 42: Control VI Block Diagram

APPENDIX D: TEST FIXTURE DRAWINGS & PROCEDURE

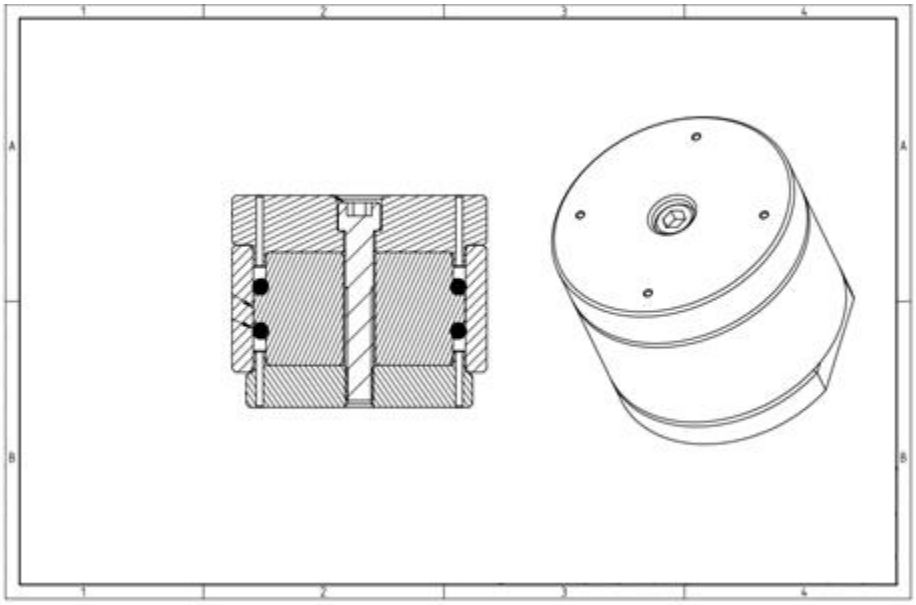

Figure 43: -223 O-ring Test Fixture

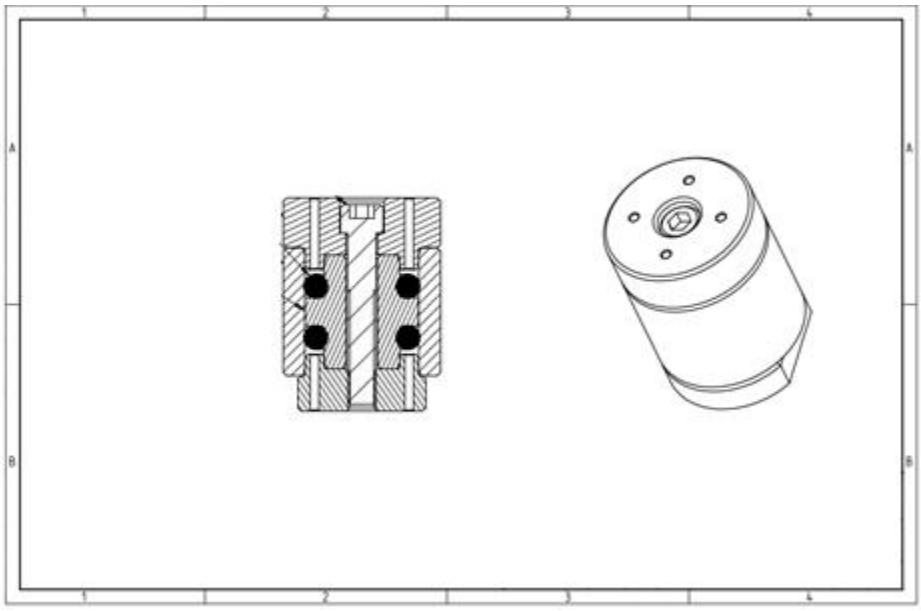

Figure 44: -312 O-ring Test Fixture

Device Assembly Procedure:

1. Ensure high pressure lines are removed, depressurization manifold mounting bolts are loosened, and pressure vessel is disassembled
2. Insert samples into pressure vessel
3. Assemble pressure vessel
    a. Insert -337 O-ring into sealing groove, use generous silicone grease
    b. Place cover on top of vessel, ensure O-ring seats properly
    c. Place thrust washer over cover
    d. Screw cap onto vessel, back off 1/8th turn once fully engaged
    e. Hand tighten all 10 set screws
    f. Tighten set screws in order to 100 ft-lbs
    g. Tighten set screws in order again to 160 ft-lbs
4. Install high pressure lines to manifolds
    a. Adjust depressurization manifold so high-pressure lines fit properly
    b. Tighten high pressure line fittings to hand tight
5. Tighten depressurization stem mounting bolts
6. Torque depressurization line fittings to 25 ft-lbs, use a ¾" wrench to back up Unions the fittings are attached to
7. Attach Thermocouple wire to pressure vessel thermocouple
8. Plug in device power cord
9. Ensure all gas supply bottles are turned on and bottle needle ball valve is opened

Device Filling Procedure

1. Open control VI on lab computer
2. Turn on VI and confirm all parameters are reading properly and valve control function is working
3. If running a heated test, start heater, confirm the heat output is 5v and temperature is rising after 5 minutes. Leave heater on for duration of testing
    a. If heater is not running, ensure "Heater Off" on page 3 of the VI is set to -200
4. Allow adequate time for vessel to reach test temperature
5. Begin filling device with gas
    a. Close "Exhaust Ball Valve"
    b. Open "Inlet Ball Valve"
    c. Turn on "Gas On" button
    d. Watch the pressure display graph, ensure pressure reaches bottle pressure
    e. Turn on "High Pressure Pump" Button
    f. Confirm pump is running by watching pressure increase in steps on the pressure graph
6. Allow pressure to increase to desired test pressure
7. Turn off "High Pressure Pump" and "Gas On" buttons in that order
8. Close "Inlet Ball Valve"
9. Open main "Fill Line Bleed" valve in the raised box on page 1 of the VI
10. Open secondary "Fill Line Bleed"

11. Close both bleed valves after an appropriate amount of time
12. Confirm pressure is holding and there are no leaks in the system by monitoring the Pressure Graph for 5 minutes
13. Allow device to dwell at test pressure for desired test dwell time

Device Depressurization Procedure

1. Return to device, make note of pressure after dwell time
2. Set "Index" on page 1 of the VI to "1"
3. Set "Heater off" valve on Page 3 of the VI to 100 psi
4. Trigger "Automatic Control" button
5. Open the "Data Acquisition" VI within the "Hardware Test" project window
6. Start "Hardware Test" VI
7. Open "Exhaust Ball Valve" to start depressurization
8. Allow depressurization of the device to 0 psi; depressurization will happen linearly based upon open loop valves calibrated to the desired depressurization rate
    a. Ensure depressurization is occurring at desired rate and "Data Acquisition" VI is operating properly, for first 5 minutes of test
9. Leave device to finish depressurizing, return after enough time for device to return to 0 psi and room temperature

Device Disassembly and Sample Removal

1. Stop "Pressure Test" VI
2. Enter room where device is located
3. Unplug the device power cord
4. Assess analog pressure gauge on device to confirm all pressure is released from the system
5. Loosen one high pressure fitting nut to allow last 10 – 20 psi of gas to escape from vessel
6. Unplug thermocouple wire
7. Loosen depressurization manifold mounting bolts
8. Loosen all high-pressure line fittings from attachment unions
9. Fully remove high pressure lines from device
10. Use large breaker bar to loosen pressure vessel set screws in a counter clockwise manner
11. Loosen set screws 1 – 2 turns by hand
12. Unscrew pressure vessel cap and lift off the device
13. Remove pressure vessel thrust washer
14. Remove pressure vessel cap, ensuring not to damage the thermocouple probe
15. Remove samples from vessel using retrieval tool
16. Allow device to sit disassembled until next test
17. Assess samples for RGD damage in desired manner

APPENDIX E: EXPERIMENTAL DATA AND ANALYSIS

Compound	Durometer	Width	Size	Compression	Temperature (°F)	Soak Time	Test Number	Samples Per	Pressure (psi)	Rate (psi/min)	Damage				Total
Buna-N	90	1/8"	-223	20.50%	75	24 hours	1	1	10,000	300	0	0	0	0	**0**
Buna-N	90	1/8"	-223	0%	75	24 hours	1	1	10,000	300	0	0	0	0	**0**
Buna-N	90	3/16"	-312	18.80%	75	24 hours	1	1	10,000	300	0	0	0	0	**0**
Buna-N	90	3/16"	-312	0%	75	24 hours	1	1	10,000	300	0	0	0	0	**0**
Buna-N	70	1/8"	-223	20.50%	75	24 hours	1	1	10,000	300	0	1	1	1	**3**
Buna-N	70	1/8"	-223	0%	75	24 hours	1	1	10,000	300	1	1	1	1	**4**
Buna-N	70	3/16"	-312	18.80%	75	24 hours	1	1	10,000	300	0	0	0	1	**1**
Buna-N	70	3/16"	-312	0%	75	24 hours	1	1	10,000	300	1	1	1	1	**4**
Buna-N	90	1/8"	-223	20.50%	250	24 hours	2	1	10,000	300	1	0	1	0	**2**
Buna-N	90	1/8"	-223	0%	250	24 hours	2	1	10,000	300	3	3	3	1	**10**
Buna-N	90	3/16"	-312	18.80%	250	24 hours	2	1	10,000	300	0	0	1	1	**2**
Buna-N	90	3/16"	-312	0%	250	24 hours	2	1	10,000	300	1	4	3	3	**11**
Buna-N	70	1/8"	-223	20.50%	250	24 hours	2	1	10,000	300	1	0	1	1	**3**
Buna-N	70	1/8"	-223	0%	250	24 hours	2	1	10,000	300	1	1	3	3	**8**
Buna-N	70	3/16"	-312	18.80%	250	24 hours	2	1	10,000	300	0	3	3	0	**6**
Buna-N	70	3/16"	-312	0%	250	24 hours	2	1	10,000	300	3	3	4	4	**14**
Viton	90	1/8"	-223	20.50%	75	24 hours	3	1	10,000	300	0	0	0	0	**0**
Viton	90	1/8"	-223	0%	75	24 hours	3	1	10,000	300	0	0	0	0	**0**
Viton	90	3/16"	-312	18.80%	75	24 hours	3	1	10,000	300	0	0	0	0	**0**
Viton	90	3/16"	-312	0%	75	24 hours	3	1	10,000	300	0	0	0	0	**0**
Viton	75	1/8"	-223	20.50%	75	24 hours	3	1	10,000	300	0	0	0	0	**0**
Viton	75	1/8"	-223	0%	75	24 hours	3	1	10,000	300	0	0	0	0	**0**
Viton	75	3/16"	-312	18.80%	75	24 hours	3	1	10,000	300	0	0	0	0	**0**
Viton	75	3/16"	-312	0%	75	24 hours	3	1	10,000	300	0	0	0	0	**0**
Viton	90	1/8"	-223	20.50%	250	24 hours	4	1	10,000	300	4	4	5	5	**18**
Viton	90	1/8"	-223	0%	250	24 hours	4	1	10,000	300	3	4	4	3	**14**
Viton	90	3/16"	-312	18.80%	250	24 hours	4	1	10,000	300	5	5	5	4	**19**
Viton	90	3/16"	-312	0%	250	24 hours	4	1	10,000	300	4	5	5	5	**19**
Viton	75	1/8"	-223	20.50%	250	24 hours	4	1	10,000	300	4	4	4	4	**16**
Viton	75	1/8"	-223	0%	250	24 hours	4	1	10,000	300	4	4	4	4	**16**
Viton	75	3/16"	-312	18.80%	250	24 hours	4	1	10,000	300	4	4	4	4	**16**
Viton	75	3/16"	-312	0%	250	24 hours	4	1	10,000	300	5	5	5	4	**19**

Table 6: Design of Experiments

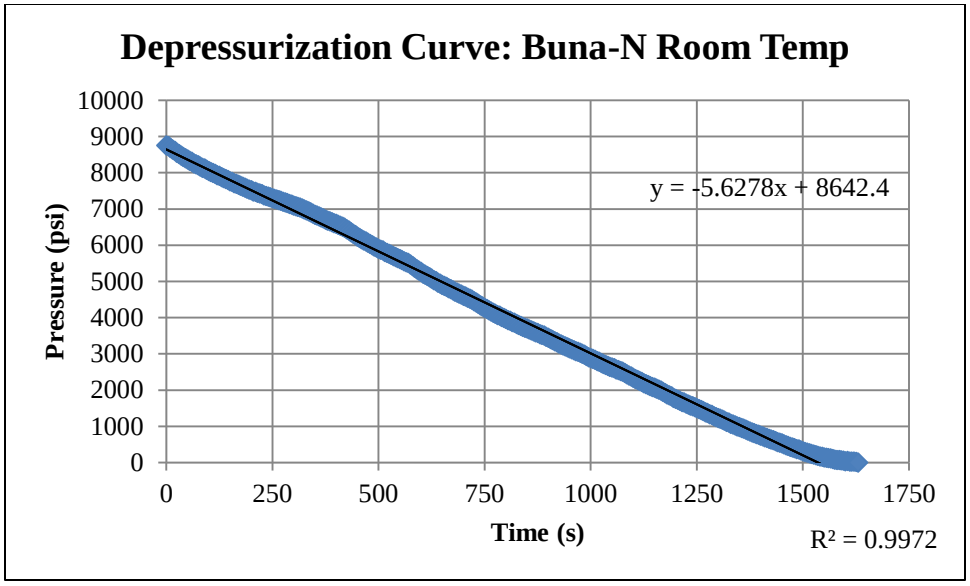

Figure 45: Depressurization Curve: Buna-N Room Temp

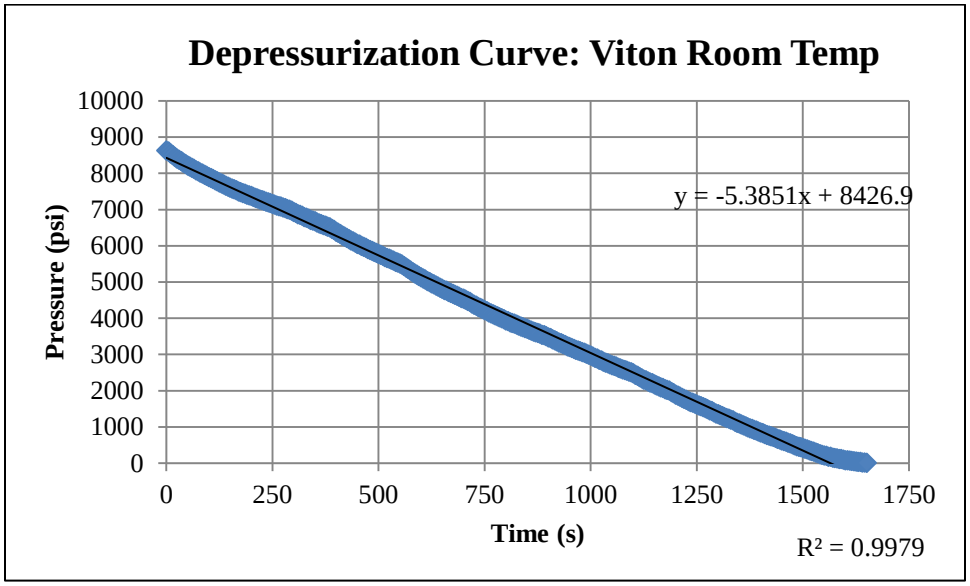

Figure 46: Depressurization Curve: Viton Room Temp

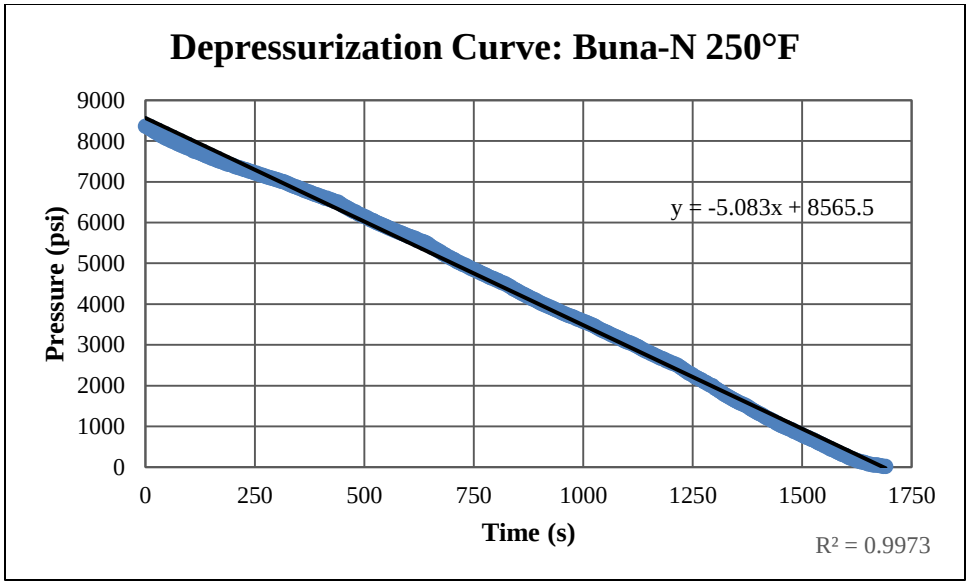

Figure 47: Depressurization Curve: Buna-N 250°F

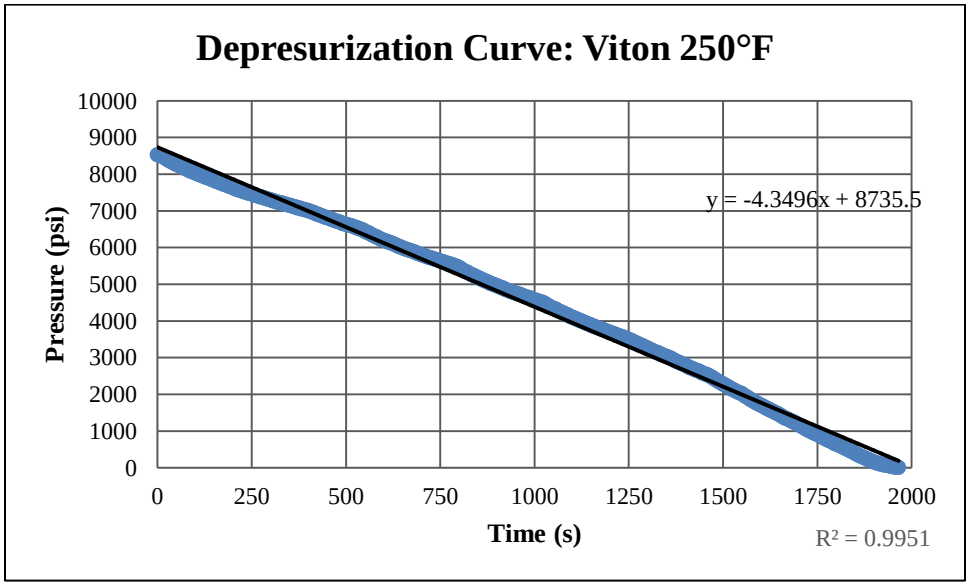

Figure 48: Depressurization Curve: Viton 250°F

REFERENCES

[1] Precicsion Polymer Engineering, “Why do O-rings fail? A brief guide to O-ring failure modes.” [Online]. Available: https://www.prepol.com/solutions/why-do-o-rings-fail-a-brief-guide-to-o-ring-failure-modes.

[2] A. K. Sevre, P. E. Smith, M. Z. Awang, M. al-Madlouh, and D. Young, “Effects of Rapid Gas Decompression on Swellable Rubber and Common Oilfield Rubber Compounds,” pp. 1–7, 2011.

[3] B. Group, “Elastomeric seals for rapid gas decompression applications in high - pressure services Prepared by BHR Group Limited for the Health and Safety Executive 2006 Elastomeric seals for rapid gas decompression applications in,” 2006.

[4] A. Stevenson and G. Morgan, “Fracture of Elastomers by Gas Decompression,” *Rubber Chemistry and Technology*, vol. 68, no. 2. pp. 197–211, 2011.

[5] B. J. Briscoe, T. Savvas, and C. T. Kelly, “‘Explosive Decompression Failure’ of Rubbers: A Review of the Origins of Pneumatic Stress Induced Rupture in Elastomers,” *Rubber Chemistry and Technology*, vol. 67, no. 3. pp. 384–416, 2011.

[6] A. Polytech, “Performance Testing.” [Online]. Available: https://www.alpinepolytech.com/index.php/testing/performance-testing.

[7] B. Schrittesser, G. Pinter, T. Schwarz, Z. Kadar, and T. Nagy, “Rapid Gas Decompression Performance of elastomers – A study of influencing testing parameters,” *Procedia Struct. Integr.*, vol. 2, pp. 1746–1754, 2016.

[8] T. H. E. Selective, P. O. F. Gases, and T. Polymers, “Permeation of Gases,” 1981.

[9] P. Wood-Adams, “Permeation in glassy polymers vs rubbery polymers,” *GCH 6101-Polymer-Diffusion*, p. 10, 2006.

[10] D. C. Weggel, “Blast threats and blast loading,” in *Blast Protection of Civil Infrastructures and Vehicles Using Composites*, Elsevier, 2010, pp. 3–43.

[11] J. M. Dealy and H. E. Park, “Effects of Pressure and Supercritical Fluids on the Viscosity of Polyethylene,” *Macromolecules*, vol. 36, no. 16, p. 5438–5452; 5438, 2006.

[12] G. J. van Amerongen, “Diffusion in Elastomers,” *Rubber Chem. Technol.*, vol. 37, no. 5, pp. 1065–1152, Nov. 1964.

[13] A. N. Gent and P. B. Lindley, “The Compression of Bonded Rubber Blocks,” *Proc. Inst. Mech. Eng.*, vol. 173, no. 1, pp. 111–122, Jun. 1959.

[14] J. Baron, K. Szklarz, and L. Macleod, “Prelimanry Results From an Automated Procedure for Explosive Decompression Evaluation of Elastomers,” 1997.

[15] J. M. Routh, “Prediction of Explosive Decompression Damage in Elastomer Seals,” 1999.

[16] B. J. Briscoe and D. Liatsis, “Internal Crack Symmetry Phenomena during Gas-Induced Rupture of Elastomers,” *Rubber Chemistry and Technology*, vol. 65, no. 2. pp. 350–373, 2011.0

[17] B. J. Briscoe and S. Zakaria, “Gas-induced damage in elastomeric composites,” *J. Mater. Sci.*, vol. 25, no. 6, pp. 3017–3023, 1990.
[18] Precicsion Polymer Engineering, “Explosive Decompression Resistant Seals.” [Online]. Available: https://www.prepol.com/industries/oil-gas/explosive-decompression.
[19] Norsok, “Qualification of Non-Metallic Sealing Materials and Manufacturers,” 1994.
[20] High Pressure Equipment Company, “High Pressure Equipment Pressure Vessels High Pressure Equipment.” [Online]. Available: https://www.highpressure.com/products/reactors-pressure-vessels/.
[21] Haskel, “Haskel-Gas-Booster-6-27-16.” [Online]. Available: https://www.haskel.com/products/gas-boosters/pneumatic-driven-gas-boosters/#downloads.
[22] Parker Autoclave Engineers, “VRMM Series MicroMetering Needle Valves.” [Online]. Available: http://www.autoclave.com/products/needle_valves/micro_metering_valves/index.html.
[23] Hanbay Electric Actuators, “Compact Valve Actuators.” [Online]. Available: http://www.hanbayinc.com/en/images/M-Series-Brochure.pdf.
[24] Omega Engeering, “High- and very-high-Temperature Pressure Transducers.” [Online]. Available: https://assets.omega.com/pdf/test-and-measurement-equipment/pressure/pressure-transducers/PX1004.pdf.
[25] Omega Engeering, “Wheatstone Bridge In-Line Signal Conditioner.” [Online]. Available: https://www.omega.com/en-us/communication-and-connectivity/signal-conditioners-and-transmitters/signal-conditioners/in-uvi-series/p/IN-UVI.
[26] Parker Autoclave Engineers, “Ball Valves 2-Way Series Ball Valves.” [Online]. Available: http://www.autoclave.com/products/ball_valves/2way_ball_valves/index.html.
[27] Parker Autoclave Engineers, “Relief valve.” [Online]. Available: http://www.autoclave.com/products/relief_valves/rvp_series/index.html.
[28] Parker Autoclave Engineers, “Accessories.” [Online]. Available: http://www.autoclave.com/aefc_pdfs/Accessories.pdf.
[29] Omega Engeering, “High Pressure Solenoid Valve.” [Online]. Available: https://assets.omega.com/pdf/valves/solenoid-valves/SVH-110.pdf.
[30] Parker Autoclave Engineers, “Needle Valves - High Pressure.” [Online]. Available: http://www.autoclave.com/products/needle_valves/high_pressure_valves_150k/index.html.
[31] B. Group, “RGD RESISTANT ELASTOMERIC SEALS.” [Online]. Available: http://www.bhrgroup.com/Default.aspx?tabid=1128.
[32] Efunda, “Design Guidelines for Radial Seals.” [Online]. Available: https://www.efunda.com/designstandards/oring/design_guidelines.cfm.